Article

Cancer Cell

Repression of Stress-Induced LINE-1 Expression Protects Cancer Cell Subpopulations from Lethal Drug Exposure

Graphical Abstract

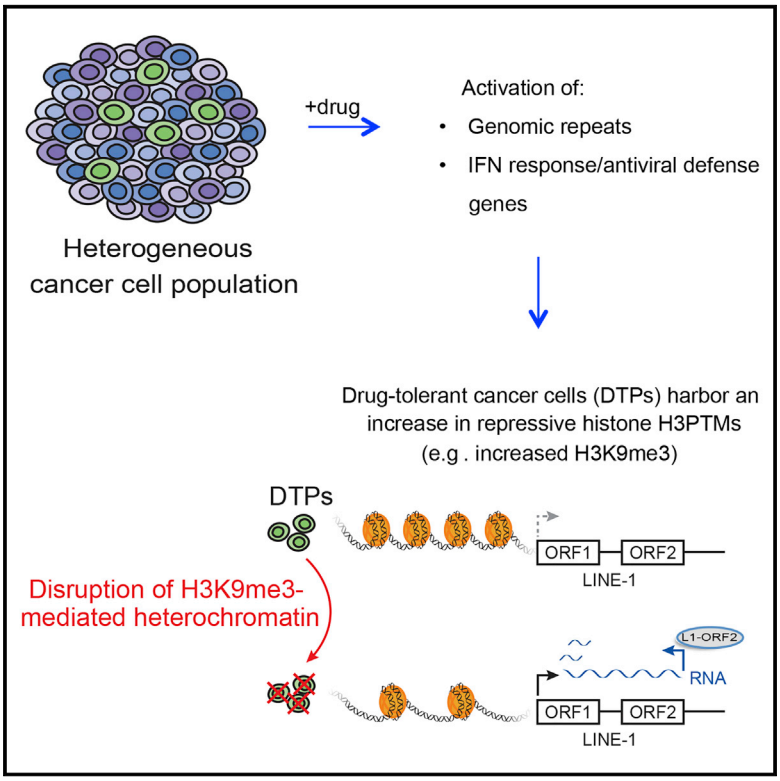

Highlights

- Drug-tolerant cancer cell subpopulations harbor a repressed chromatin state
- Disruption of the repressed chromatin state is lethal to drug-tolerant cancer cells
- Drug exposure induces expression of repeat elements and interferon-stimulated genes
- Survival of drug-tolerant cells requires increased H3K9me3 over LINE-1 elements

Authors

Gulfem Dilek Guler, Charles Albert Tindell, Robert Pitti, ..., Jean-Philippe Stephan, David Arnott, Marie Classon

Correspondence

classon.marie@gmail.com

In Brief

Guler et al. show that drug-tolerant persisters (DTPs), a cancer cell subpopulation surviving lethal drugs, are partly maintained by a repressed chromatin state, prominently at LINE-1 elements. Disrupting the repressive chromatin results in death of DTPs, which is partially rescued by reducing LINE-1 expression.

Guler et al., 2017, Cancer Cell *32*, 1–17
August 14, 2017
http://dx.doi.org/10.1016/j.ccell.2017.07.002

CellPress

Please cite this article in press as: Guler et al., Repression of Stress-Induced LINE-1 Expression Protects Cancer Cell Subpopulations from Lethal Drug Exposure, Cancer Cell (2017), http://dx.doi.org/10.1016/j.ccell.2017.07.002

Cancer Cell
Article

Repression of Stress-Induced LINE-1 Expression Protects Cancer Cell Subpopulations from Lethal Drug Exposure

Gulfem Dilek Guler,[1,9] Charles Albert Tindell,[1,9] Robert Pitti,[1] Catherine Wilson,[1] Katrina Nichols,[2] Tommy KaiWai Cheung,[2] Hyo-Jin Kim,[1] Matthew Wongchenko,[4] Yibing Yan,[4] Benjamin Haley,[5] Trinna Cuellar,[5] Joshua Webster,[6] Navneet Alag,[1] Ganapati Hegde,[1] Erica Jackson,[1] Tracy Leah Nance,[7] Paul Garrett Giresi,[7] Kuan-Bei Chen,[8] Jinfeng Liu,[3] Suchit Jhunjhunwala,[3] Jeff Settleman,[1,11] Jean-Philippe Stephan,[2,10] David Arnott,[2] and Marie Classon[1,*]

[1]Molecular Oncology, Genentech Inc., 1 DNA Way, South San Francisco, CA 94080, USA
[2]Protein Chemistry, Genentech Inc., South San Francisco, CA, USA
[3]Bioinformatics, Genentech Inc., South San Francisco, CA, USA
[4]LS Biomarker Development, Genentech Inc., South San Francisco, CA, USA
[5]Molecular Biology, Genentech Inc., South San Francisco, CA, USA
[6]Pathology, Genentech Inc., South San Francisco, CA, USA
[7]Epinomics, Menlo Park, CA, USA
[8]Active Motif, Carlsbad, CA, USA
[9]These authors contributed equally
[10]Present address: Institut de Recherche Servier, 125 Chemin de Ronde, Croissy-sur-Seine 78290, France
[11]Present address: Calico Life Sciences, 1170 Veterans Blvd, South San Francisco, CA 94080, USA
*Correspondence: classon.marie@gmail.com
http://dx.doi.org/10.1016/j.ccell.2017.07.002

SUMMARY

Maintenance of phenotypic heterogeneity within cell populations is an evolutionarily conserved mechanism that underlies population survival upon stressful exposures. We show that the genomes of a cancer cell subpopulation that survives treatment with otherwise lethal drugs, the drug-tolerant persisters (DTPs), exhibit a repressed chromatin state characterized by increased methylation of histone H3 lysines 9 and 27 (H3K9 and H3K27). We also show that survival of DTPs is, in part, maintained by regulators of H3K9me3-mediated heterochromatin formation and that the observed increase in H3K9me3 in DTPs is most prominent over long interspersed repeat element 1 (LINE-1). Disruption of the repressive chromatin over LINE-1 elements in DTPs results in DTP ablation, which is partially rescued by reducing LINE-1 expression or function.

INTRODUCTION

Drug tolerance within subpopulations of heterogeneous cells presents a substantial impediment to successful drug treatment in various pathological contexts, including bacterial infections and cancer. In bacteria, a relatively quiescent subpopulation of antibiotic-resistant cells, referred to as "persisters" (Balaban et al., 2013; Holden, 2015), exhibits reversible and transient drug-tolerant properties. This population has been implicated in a "bet-hedging" strategy that ensures population survival. In the face of potentially harmful fluctuating environments, such a mechanism obviates the requirement for extensive genome mutations, which are irreversible and can potentially reduce "fitness" (Darmon and Leach, 2014; de Jong et al., 2011). In the context of cancer, innate and acquired drug resistance remains a major limitation to the efficacy of all therapies.

Significance

Drug-resistant cell populations within heterogeneous tumors can serve as the founders of disease relapse, which remains a major impediment to successful cancer treatment. Our findings establish a paradigm wherein epigenetic repression of highly repetitive genome elements contributes to the survival of a so-called "drug-tolerant" subpopulation of cancer cells by serving as a counterbalance to drug-induced expression of these elements as well as antiviral defense networks. Such a balance promotes genomic stability and fitness in this cancer cell subpopulation during otherwise lethal drug exposures. These observations reveal a potential opportunity to disrupt the drug-tolerant state to more effectively suppress the acquired resistance to anti-cancer drugs that is frequently observed in the clinic.

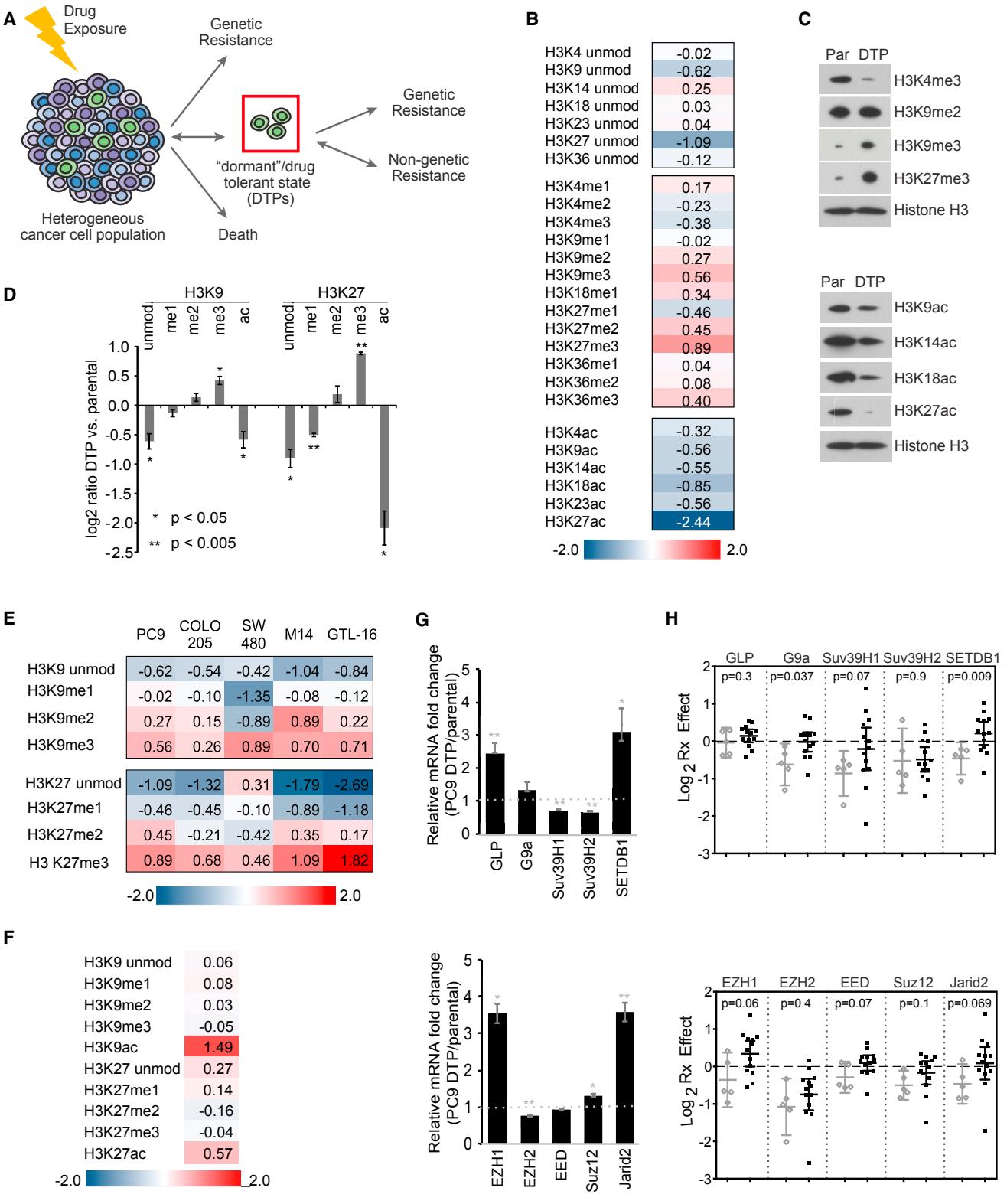

Figure 1. Increase in Histone H3K9 and K27 Methylation in DTP Populations

(A) Schematic representation of heterogeneous responses to drugs in cancer cells. DTPs are largely quiescent, reversibly tolerant to drug exposure, and serve as the founder population for various acquired drug resistance mechanisms.

(B) Differences in the relative abundance of H3PTMs between PC9 cells and PC9DTPs (log_2 ratios DTP versus PC9). A representative experiment is shown.

(C) Immunoblots using antibodies against various H3PTMs in PC9 parental cells (Par) and PC9-derived DTP extracts.

(legend continued on next page)

We previously identified a largely quiescent cancer cell subpopulation that transiently survives lethal drug exposures, drug-tolerant persisters (DTPs) (Sharma et al., 2010). These cells serve as founders for disease relapse that can occur through mutational and non-mutational mechanisms (Figure 1A) (Groenendijk and Bernards, 2014; Hata et al., 2016; Kuczynski et al., 2013; Ramirez et al., 2016). DTPs arise from a dynamically fluctuating cell population that displays characteristics of cancer stem cells and altered metabolism (Raha et al., 2014; Roesch et al., 2010), and the reversible character of the DTP state (Sharma et al., 2010) implicates epigenetic mechanisms in their survival. Epigenetic regulatory mechanisms play crucial roles in many aspects of biology and allow cells to respond to signals that determine fate specification and genome stability during development (Allis and Jenuwein, 2016; Cantone and Fisher, 2013), and provides organisms with mechanisms to adapt to environmental changes (Feil and Fraga, 2011). Here, we have undertaken a multifaceted investigation of the molecular mechanisms underlying DTP survival.

RESULTS

Drug-Tolerant Cancer Cells Exhibit Distinct Histone Tail Modifications

To evaluate changes in the chromatin structure of DTPs (Figure 1A, red box) relative to the heterogeneous tumor cell population, we first measured histone H3 post-translational modifications (PTMs) by mass spectrometry (MS) (Maile et al., 2015). In the *EGFR*-mutant non-small-cell lung cancer (NSCLC) cell line PC9 and corresponding DTPs generated using the EGFR kinase inhibitor erlotinib (erl), we observed a global decrease in acetylation of H3 lysines (H3KAc) in DTPs (Figure 1B; Table S1). In addition to the global decrease in H3KAc and a previously described reduction in tri-methylation of H3 lysine 4 (H3K4me3) in DTPs (Vinogradova et al., 2016), this analysis revealed several additional repressive H3PTM changes (Figure 1B; Table S1), verified by immunoblotting (Figure 1C). Most significantly, H3K9 and H3K27 methylation was increased in PC9DTPs (Figure 1D), as well as in DTPs derived from multiple other cancer cell line models (Figure 1E). The MS and immunoblotting findings were further supported by immunohistochemistry in residual cancer cells following drug-induced tumor regression *in vivo* (Figures S1A and S1B). The global H3PTM changes in PC9DTPs are transient, and PC9DTEPs (drug-tolerant expanded persisters) as well as PC9DTPs, allowed to re-grow following drug removal, no longer harbor most of these alterations (Figure S1C).

DTPs originate in a stochastically fluctuating population of cells that express aldehyde dehydrogenase (ALDH) (Raha et al., 2014). To investigate whether the repressive H3PTMs in DTPs pre-exist in the subpopulation that shows increased ALDH expression, we used fluorescence-activated cell sorting (FACS) to separate drug-naive PC9 cells into $ALDH^{high}$ and $ALDH^{low}$ fractions (Figure S1D). Histone MS analysis of these fractions revealed that the repressive state did not pre-exist in the $ALDH^{high}$ population of cells. Rather, this population displayed a slight increase in activating PTMs such as H3K9Ac and H3K27Ac, and these modifications were reduced in the $ALDH^{high}$ population after drug exposure (Figures 1F and S1E; Table S1). Altogether, these results show that DTPs exhibit an increase in global repressive histone H3PTMs that do not exist in the $ALDH^{high}$ subpopulation prior to drug exposure.

Increased Expression of H3K9 Methyltransferases in Drug-Regressed Tumors

To explore a possible role of H3K9 and K27 methylation in DTP survival, we analyzed expression of components of histone methyltransferase complexes involved in their methylation in DTPs from several cell line models and in drug-regressed patient-derived tumor samples. The cell line data showed increased expression of H3K9 methyltransferases, as well as some H3K27 methyltransferase components in PC9-derived DTPs, and in DTPs derived from various other cell line models (Figures 1G, S1F, and S1G). We then analyzed the expression of these genes in pre- and on-vemurafenib treatment biopsies from B-RAFV600E mutant melanoma patients, and observed an expression pattern in the drug-regressed tumor samples similar to that observed in DTPs *in vitro* (Figure 1H and Table S2). The most significant change in the patient samples was in the expression of the H3K9 methyltransferase SETDB1/ESET/KMT1E, which was increased in on-treatment biopsies from some patients whose tumors responded to drug (Figure 1H, black dots). In contrast, SETDB1 expression did not increase in on-treatment biopsies from treatment-refractory patients (Figure 1H, gray dots). A strong correlation between the increased expression of SETDB1 and G9a/EHMT2/KMT1C was also observed in on-treatment biopsies from responding patients (Figure S1H; Table S2). Together with the histone H3PTM changes, these results suggest an involvement of H3K9 methyltransferases and increased H3K9 methylation in DTP survival.

(D) Differences in the relative abundance of H3K9 and K27 PTMs between PC9 and PC9DTPs (log_2 ratios). The data presented are based on the analysis of three independent biological replicates, and error bars represent ±SD of the log_2 values comparing DTPs with PC9s, and p values were generated using paired t test on log_2-transformed relative abundances.

(E) Histone MS analysis of H3K9 and K27 methylation in several DTP models compared with their respective parental population (log_2 ratios DTPs versus parental populations).

(F) Histone MS analysis of drug-naive FACS-sorted $ALDH^{high}$ compared with the $ALDH^{low}$ PC9 subpopulations (log_2 ratios $ALDH^{high}$ versus $ALDH^{low}$).

(G) Relative fold changes in mRNA levels of H3K9 (upper panel) and H3K27 (lower panel) methyltransferase components in PC9DTPs compared with the PC9 parental population. Ct values were normalized to GAPDH, ±SD calculated based on the fold change in triplicate from two independent experiments and p values were generated using unpaired t test.

(H) Expression changes of H3K9 and K27 methyltransferase components, as measured by nanostring, in on-vemurafenib treatment tumor biopsies as compared with pre-treatment biopsies from the same patient. The patients (n = 18, BRIM-2 trial) were categorized as best objective RECIST response of progressive disease/stable disease (PD/SD, gray dots) and patients with a partial response (PR, black dots), and p values were generated using t test (not assuming equal variance) comparing the PR with the PD/SD group. Error bars represent 95% confidence intervals.

*$p < 0.05$, **$p < 0.01$. See also Figure S1 and Tables S1 and S2.

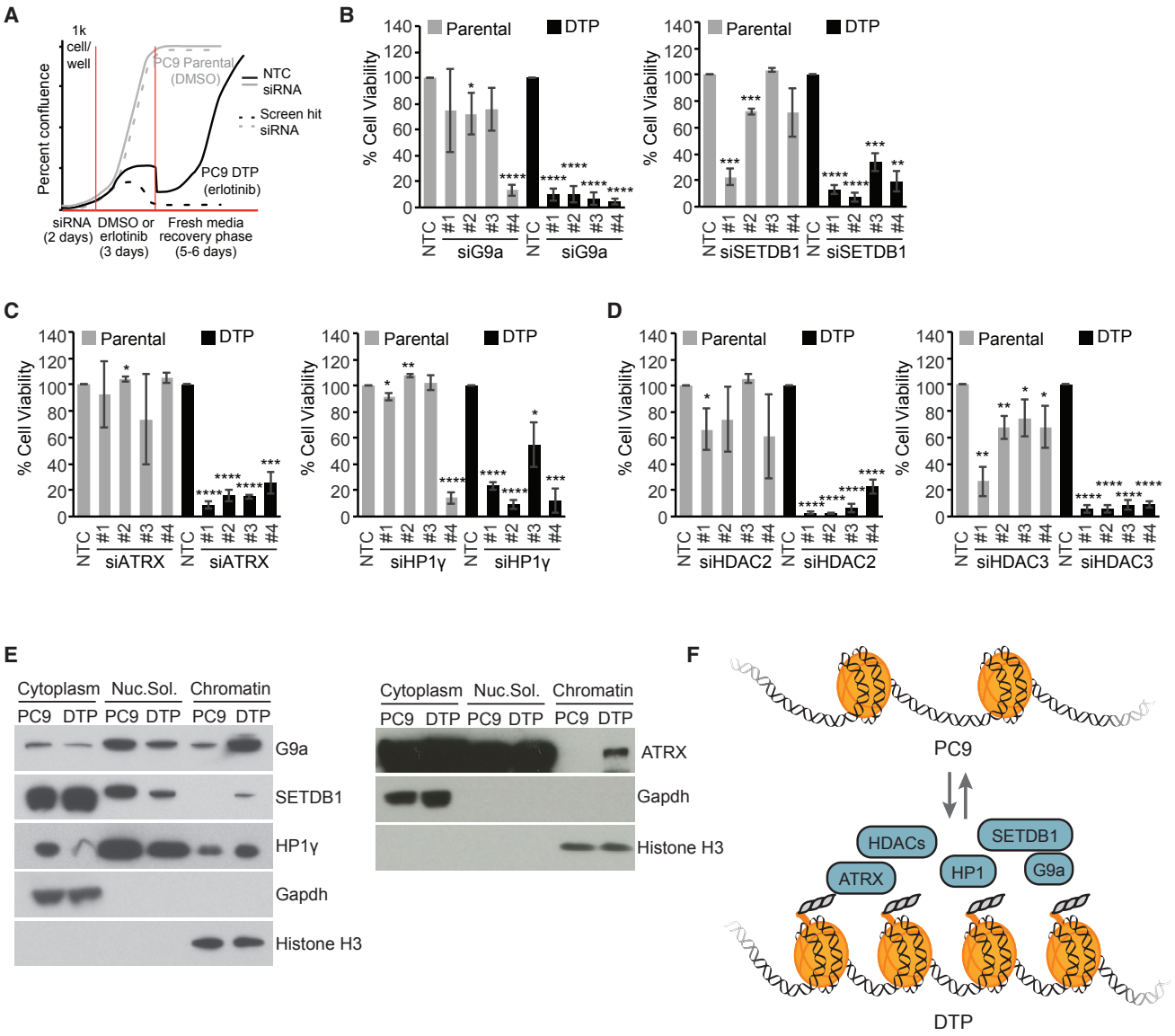

Figure 2. siRNA Screen Reveals a Role for H3K9 Methylation-Mediated Heterochromatin Formation in DTP Survival

(A) Schematic representation of the siRNA screen format designed to identify chromatin-modifying gene products required for DTP survival. Gray lines represent parental cells and the black line represents DTPs, in each case the dotted lines represent a screen hit compared with the non-targeting control (NTC, solid line).

(B–D) Effect of siRNAs targeting G9a and SETDB1 (B), ATRX and HP1γ (C), and HDAC2 and HDAC3 (D) on parental (gray bars) and DTP (black bars) populations. The screen was run twice in duplicate and error bars represent ±SD of the fold changes of each siRNA (n = 4, 2 for each screen) compared with the NTC (n = 16, 8 from each screen run on several plates) for each experiment and p values were generated using paired t test.

(E) Immunoblots showing protein levels of G9a, SETDB1, ATRX, and HP1γ in the cytoplasmic, nuclear-soluble, and chromatin-enriched fractions obtained from PC9 and PC9DTPs. GAPDH and histone H3 were used as loading and fractionation controls. A representative experiment is shown.

(F) Graphic summary of DTP siRNA screen hits related to H3K9me3-mediated heterochromatin formation. Illustrated in the figure is also the reversible increase in heterochromatin observed in DTPs.

*p < 0.05, **p < 0.01, ***p < 0.001, ****p < 0.0001. See also Figure S2 and Tables S3 and S4.

DTP Survival Requires Gene Products that Promote H3K9me3-Mediated Heterochromatin

To directly explore DTP vulnerabilities related to their altered chromatin state, we performed a small interfering RNA (siRNA) screen (Figure 2A). We used an arrayed library of siRNAs corresponding to 298 genes (4 siRNA/gene) whose products function in chromatin regulation (Table S3). Two days after PC9 cells were transfected with each siRNA, cells were treated with a vehicle control (DMSO) or 1 μM erl for 3 days, at which time the drug-treated population was largely reduced. The surviving cells were quantified following re-growth in the absence of erl for 5 days (Figure 2A). Screens for which the readout is increased lethality often suffer from a high false-positive rate, since many siRNAs are broadly cytotoxic (Table S3). Therefore, we scored

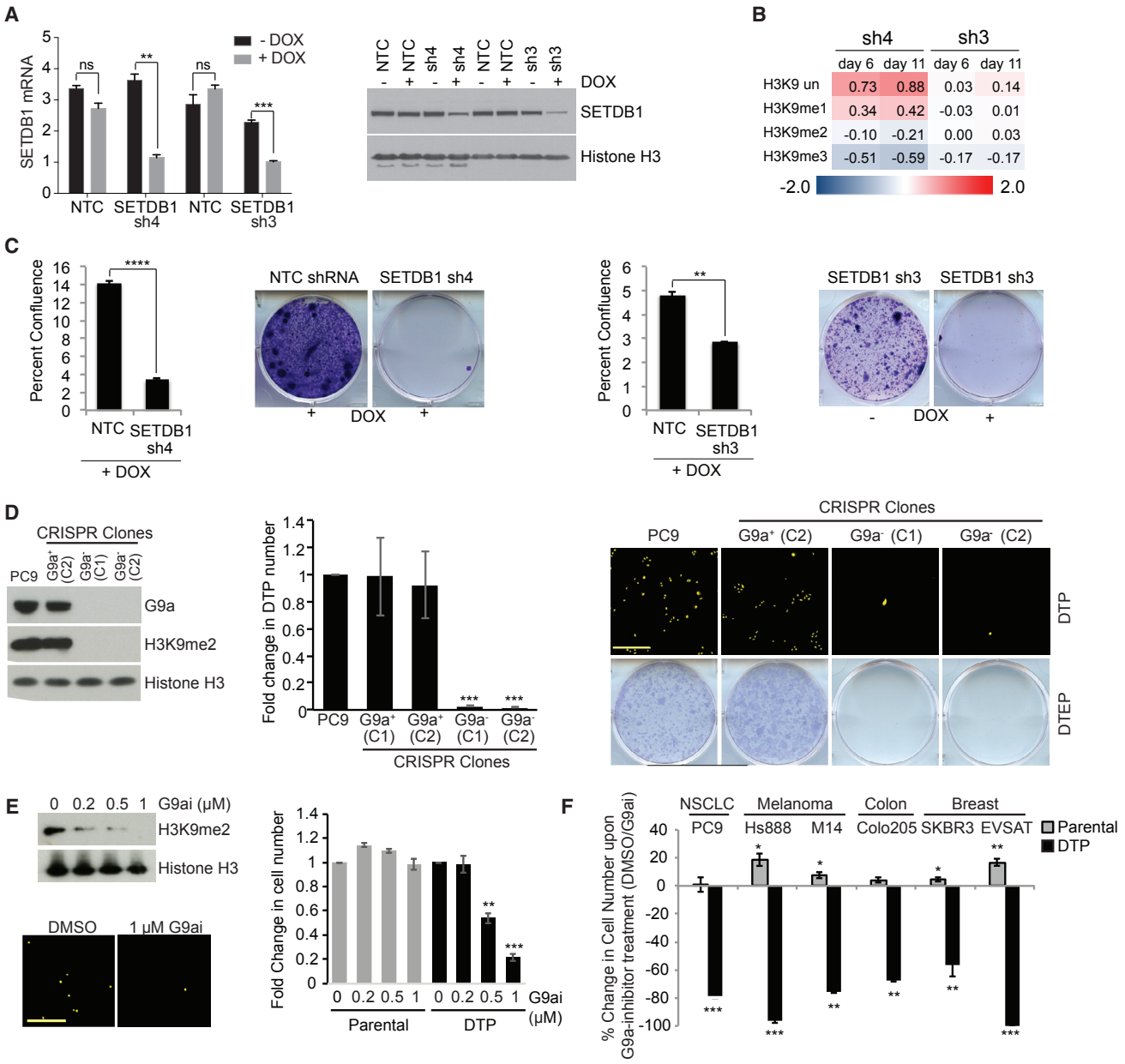

Figure 3. H3K9 Methyltransferases Are Required for Establishment of the Drug-Tolerant State

(A) SETDB1 expression in SW480 cell line pools expressing doxycycline (DOX)-inducible shRNAs directed against SETDB1 (SETDB1-sh3 and SETDB1-sh4) compared with the NTC following 3 days in DOX (250 ng/mL). The RNA analysis (left) was run in triplicate using β-actin as the internal control. The error bars represent ±SD, and p values were calculated using paired t test. A representative example of protein analysis (right) is shown.

(B) Histone MS analysis of H3K9 modification changes in the presence of DOX (250 ng/mL) for 6 or 11 days in the SETDB1-sh3 and -sh4 clones compared with DOX-treated NTC control (log_2 ratios are shown).

(C) The effect of decreased expression of SETDB1 (250 ng/mL DOX for 5 days prior to addition of chemotherapeutic agents 5-FU and SN38) on the number of SW480 DTPs following treatment with 5-FU and SN38 compared with DMSO-treated cells expressing DOX-inducible NTC-sh. Remaining cells were analyzed by IncuCyteZoom, ± SD was calculated from the average number of cells per image per well in triplicate based on two independent experiments, and p values were calculated using paired t test. The panels to the right of the graphs show a representative example of Giemsa-stained dishes, following 40 days of re-growth in the absence of drugs following 14 days of 5-FU and SN38 treatment.

(D) Immunoblot analysis showing G9a and H3K9me2 levels in clone 1 (C1) and clone 2 (C2) where the EHMT2/G9a gene was disrupted by CRISPR ($G9a^-$) or a selected CRISPR clone still expressing G9a ($G9a^+$), with histone H3 as loading control (left) and the effect of G9a loss on the survival of PC9DTPs in the two clones ($G9a^-$ C1 and C2, right). Changes in the number of PC9DTPs were measured using IncuCyteZoom imaging, error bars represent ±SD in fold change in two independent experiments performed in triplicate, and p values were calculated compared with parental PC9 cells using paired t test. The right panel shows representative images of nuclear red cells (pseudo-colored yellow), PC9DTPs. Scale bar, 800 μm (upper panels) or Giemsa-stained dishes showing colonies formed after 30 days in erl (DTEPs, bottom panels).

(legend continued on next page)

only those genes for which at least three of four siRNAs decreased DTP cell numbers while minimally affecting the parental PC9 population.

Consistent with the observed increased H3K27 methylation, several H3K27 methyltransferase components scored weakly in the siRNA screen (Figure S2A and Table S3). Notably, EZH2 has previously been implicated in drug resistance in the context of Notch inhibition (Knoechel et al., 2014). CRISPR-mediated deletion of *EZH2*, or treatment with EZH2 inhibitors (EZH2i, EPZ-6438, and GSK12) also reduced the number of DTPs (Figures S2B–S2G, black bars) at concentrations of EZH2i that minimally affected the heterogeneous parental PC9 population (Figures S2E–S2G, gray bars).

The siRNA screen also identified several genes whose products are involved in H3K9 methylation-dependent heterochromatin formation. For example, siRNAs targeting the H3K9 methyltransferases SETDB1 and G9a (Figure 2B; Table S3), the methyl-reader proteins heterochromatin protein-1 gamma (HP1γ), and ATRX (Figure 2C; Table S3), as well as several class I HDACs (Figure 2D; Table S3), reduced the number of DTPs.

ATRX, in complex with DAXX, deposits the histone H3 variant H3.3 in heterochromatic genomic regions (Filipescu et al., 2014), and H3.3 levels were increased in multiple DTP models (Figure S2H) as well as in drug-regressed PC9 tumors *in vivo* (Figure S2I). Following chromatography separation of H3 variants, an MS analysis showed that H3.3 in DTPs harbored mostly repressive modifications (Figures S2J–S2L; Table S4). Moreover, reduced expression of H3.3 resulted in a DTP decrease (Figures S2M and S2N), confirming a role for ATRX in DTP survival. ATRX contains a shared domain with the *de novo* DNA methyltransferases DNMT3 A, B, and L (Noh et al., 2016). This domain preferentially binds to histone peptides containing unmodified H3K4 and H3K9me3 (Iwase et al., 2011), an H3 methylation signature found in DTPs (Table S1). Although the *de novo* DNA methyltransferases did not score in the siRNA screen (Table S3), DNMT3L protein was increased in DTP chromatin compared with the parental chromatin fraction (Figure S2O) and low doses of the DNMT inhibitor 5-azacytidine blocked the transition of DTPs into proliferating DTEPs (Figures S2P and S2Q), suggesting a role for this group of proteins in the propagation of the drug-tolerant state.

In addition to ATRX, we found that depletion of another H3K9me3 binding protein, HP1γ, reduced DTPs (Figure 2C and Table S3). Studies in *S. pombe* suggest that H3K9 methylation and HP1 proteins serve as recruiting platforms for factors involved in heterochromatin silencing, including HDACs (Aygun et al., 2013). Notably, depletion of HDACs 2 and 3 also reduced DTPs in the siRNA screen (Figure 2D and Table S3), consistent with previous findings that DTPs are more sensitive to the class I HDAC inhibitor trichostatin A (TSA) (Sharma et al., 2010). In addition, more specific pharmacologic inhibitors of HDAC1/2 or HDAC3 reduced DTPs (Figure S2R), and serial salt extractions showed that HDACs 2 and 3 were localized to more heterochromatic regions in DTPs (Figure S2S). Furthermore, G9a, SETDB1, HP1γ, as well as ATRX proteins, were enriched in the chromatin fraction of PC9DTPs (Figure 2E). Together, these results suggest a general requirement for factors involved in the propagation of H3K9 methylation-dependent heterochromatin in the establishment of the drug-tolerant state (Figure 2F).

Reduced Expression or Activity of SETDB1 and G9a Results in Less DTPs

To further confirm a role for the H3K9 methyltransferases in DTP survival, we used knockout and knockdown (KD) approaches as well as a G9a inhibitor (UNC-0638) (Vedadi et al., 2011). First, we introduced doxycycline (DOX) inducible short hairpins (sh) to reduce the expression of SETDB1 in the colorectal tumor cell line SW480, from which DTPs displayed the greatest increase in H3K9me3 (Figure 1E). Cells expressing SETDB1 shRNAs showed a reduction in SETDB1 expression and varying degrees of reduction H3K9me3 upon DOX induction (Figures 3A and 3B). Treatment with chemotherapeutic agents (fluorouracil [5-FU] and 7-ethyl-10-hydroxycamptothecin [SN38]) following 5 days of DOX exposure revealed a requirement for SETDB1 in SW480DTP survival (Figure 3C).

Next, to validate a role for G9a in the establishment of PC9DTPs, we used the CRISPR/Cas9 system to disrupt the expression of G9a in PC9 cells. Clones that show no expression of G9a (G9a^{-}) showed a decrease in H3K9me1/2 (Figures 3D and S3A), and demonstrated a reduction in DTP numbers rescued by G9a re-expression (Figures 3D and S3B). PC9 cells were unaffected by loss of G9a expression at early passage, but these cell populations displayed reduced tumor re-initiation potential *in vivo* (Figure S3C), a property shared by cancer stem cells. Treatment of PC9 cells with UNC-0638, a pharmacologic inhibitor of G9a and its related methyltransferase GLP, also decreased H3K9me1/2 with a subtle effect on H3K9me3 (Figures 3E and S3A). As in cells that have lost the G9a protein (G9a^{-}), pre-treatment with UNC-0638 specifically reduced PC9DTPs in a dose-dependent manner (Figure 3E) as well as in several other DTP cell line models (Figures 3F and S3D). Collectively, these findings confirm a broad role for H3K9 methyltransferases in DTP survival.

Repressive Chromatin State in DTPs Does Not Correlate with a General Decrease in the Expression of Uniquely Mapping Genes

To further define a role for the repressive chromatin state in DTPs, we performed RNA sequencing (RNA-seq). Surprisingly, the analysis of the RNA-seq data showed a general increase in

(E) PC9 cells were treated with indicated concentrations of UNC-0638 (G9ai) for 5 days prior to treatment with erl. Effect of UNC-0638 treatment on H3K9me2 (upper left) and DTPs (representative images where the cells are pseudo-colored yellow). Scale bar, 800 μm (bottom left) and quantified changes in DTP numbers (bargraph) following treatment with the indicated concentrations of UNC-0638 compared with DMSO control for parental PC9 cells (gray bars) and PC9DTPs (black bars). Shown is a representative dose-response experiment (n = 3), error bars represent ±SD, and p values were generated using paired t test.

(F) Percent change in the number of parental (gray bars) or DTP cells (black bars) upon treatment with 1 μM UNC-0638 (G9ai) in PC9, Hs888, M14, Colo205, SKBR3, and EVSAT cell line models. All cell numbers were quantified using IncuCyteZoom; ±SD was calculated from the average number of cells per image per well in triplicate, and p values were calculated with paired t test.

ns > 0.05, *p < 0.05, **p < 0.01, ***p < 0.001, ****p < 0.0001. See also Figure S3.

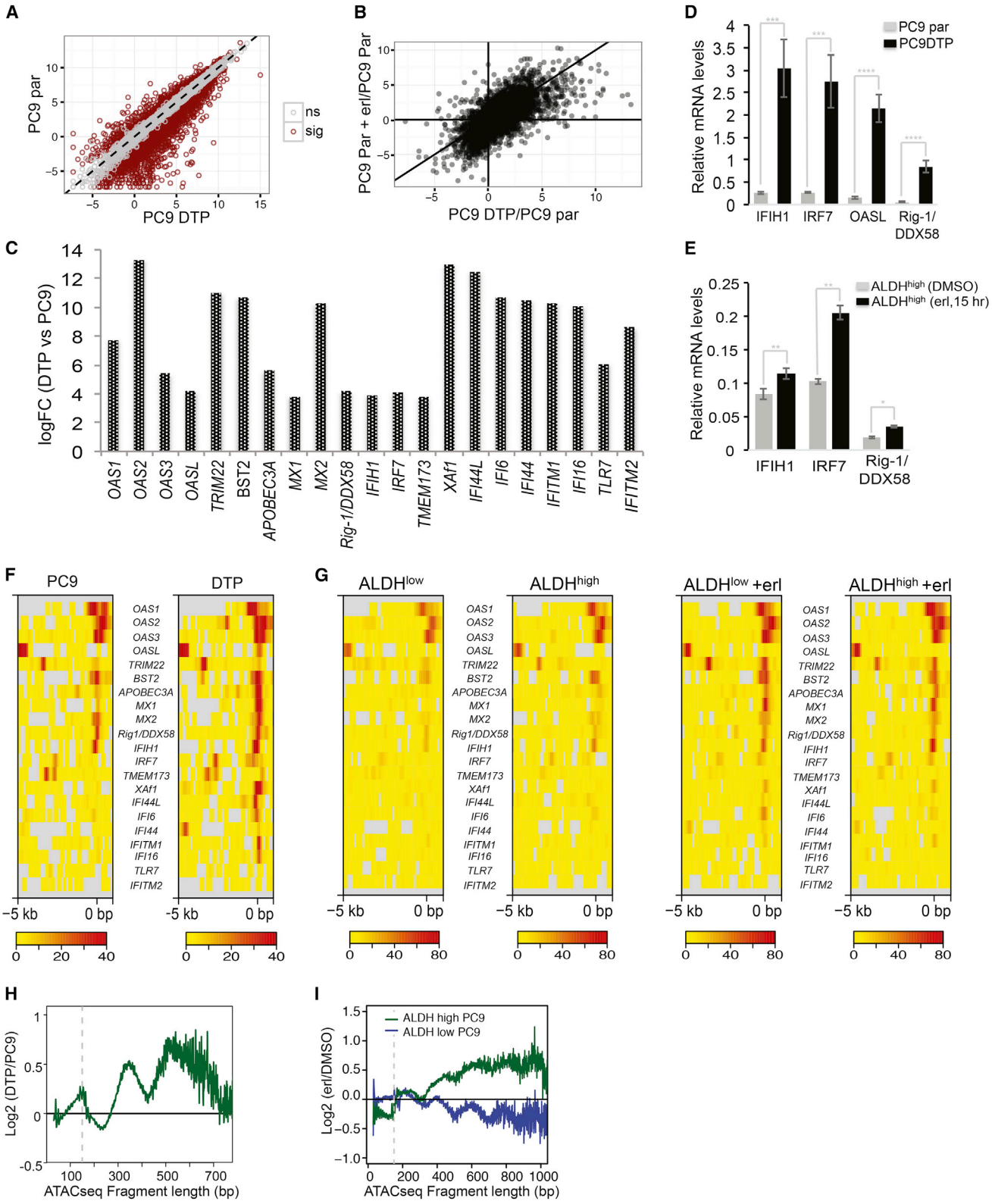

Figure 4. DTPs Display an Antiviral Defense Signature

(A) RNA-seq analysis showing average gene expression in PC9DTPs compared with the parental (par) PC9 population. Shown in red are the significant changes in gene transcription from three independent experiments normalized to an ERCC spike-in control (added based on cell number) (BH-adjusted p value ≤ 0.05, from differential expression analysis using the voom-limma approach).

(legend continued on next page)

unique gene transcription in PC9DTPs compared with the bulk PC9 population (Figures 4A and 4B; Table S5). Among the most induced genes in PC9DTPs were a large number of interferon (IFN) response/antiviral defense genes (Figures 4C and 4D; Table S5). Many of these genes were also induced in the parental population following short-term exposure to erl or carboplatin (Table S5; Figure 4E). Increased expression of IFN response/antiviral defense genes in tumor cells can result from transcriptional increases in genomic repeat regions (Roulois et al., 2015; Chiappinelli et al., 2015), and we found transcription of many repeat elements to be induced by erl or carboplatin in PC9 cells (Table S6). Consistent with the RNA-seq analysis, an assay for transposase-accessible chromatin combined with high-throughput sequencing (ATAC-seq) (Buenrostro et al., 2015) showed a general increase in the accessibility (more peaks) in genes that show increased expression in DTPs, including IFN response genes in DTPs and in the drug-treated ALDH^{high} population of cells (Figures S4A and S4B). Furthermore, the regulatory regions of IFN response/antiviral defense genes also showed an increase in the ATAC-seq signal specifically in DTPs (Figures 4F and S4C). Although the ATAC-seq signals in the promoter regions of these genes were slightly higher in the drug-naive ALDH^{high} population (Figure S4D), erl exposure resulted in increased transposase accessibility (ATAC-seq reads) in the promoter regions of IFN response/antiviral defense genes in the ALDH^{high} as well as the ALDH^{low} populations (Figures 4G and S4D). Together, these findings reveal a drug-induced expression of repeat elements and IFN response/antiviral response genes in the heterogeneous cancer cell population.

Consistent with the repressive H3PTMs a further analysis of the ATAC-seq data revealed an overall increase in the number of longer ATAC-seq fragments in the PC9DTPs, indicative of an increase in less-accessible regions in their genomes (Figures 4H and S4E). A similar increase in longer ATAC-seq reads was seen in the ALDH^{high}, but not the ALDH^{low}, population following erl exposure (Figures 4I and S4F). Consistent with the MS analysis (Figure 1F; Table S1) the ATAC-seq analysis indicated that the ALDH^{high} population did not display an increase in longer ATAC-seq reads compared with the ALDH^{low} population prior to drug exposure (Figure S4G). Collectively, these studies suggest that the drug-induced increased expression of genomic repeat elements and IFN response/antiviral defense genes is accompanied by a global increase in repressive chromatin that most likely reside outside of uniquely mapping gene regions in DTPs.

H3K9 Methylation Accumulates over LINE-1 Elements in Drug-Tolerant Cancer Cells

Given the requirement for factors involved in H3K9me3-mediated heterochromatin formation in DTP survival and previous studies demonstrating that H3K9me3 is primarily localized to repetitive regions of the genome (Barski et al., 2007; Mikkelsen et al., 2007), we next investigated where the observed global H3K9me3 increases reside in DTP genomes by chromatin immunoprecipitation followed by sequencing (ChIP-seq). The H3K9me3-ChIP-seq analysis led to the identification of 45,442 H3K9me3-enriched regions in the PC9DTP chromatin compared with 23,082 regions in the PC9 parental chromatin (Figures 5A and S5A). The number of reads within H3K9me3 peaks was also specifically increased in the DTPs (Figure 5B). An annotation of H3K9me3-enriched regions against gene and repeat features in the human genome showed an increase in both uniquely mapping gene and repeat regions, including centromeric and telomeric repeats, in chromatin from DTPs (Figures S5B and S5C). Further analysis of the H3K9me3-ChIP-seq data showed that the distribution over gene features was similar when chromatin from DTP and parental populations was compared (Figure 5C, upper panel). In contrast, an analysis of the distribution over repeat elements showed an increased accumulation of H3K9me3 over LINE-1 elements in chromatin from PCDTPs (Figure 5D, lower panel).

LINE-1-derived sequences account for approximately 1/5 of the human genome (Goodier and Kazazian, 2008; Hancks and Kazazian, 2012). The majority of the human LINE-1 elements are degenerated, truncated, and mutated transposition remnants, but approximately 7,000 elements remain as full-length LINE-1s. These elements encode three open reading frames, referred to as ORF0, 1, and 2, and some retain the ability to retrotranspose. K-means clustering of the LINE-1s occupied by H3K9me3 in the chromatin from PC9 and PC9DTPs indicated coverage throughout the elements (Figures 5E, S5D, and S5E), as well as a general increase in H3K9me3 over these elements in DTPs. A further comparison of sequence-length distributions of all LINE-1 copies found in the human genome assembly 19 with the H3K9me3-enriched LINE-1s showed that H3K9me3 is mostly enriched over longer LINE-1 copies (Figure 5F), including the primate-specific families L1PA2-6 and the human-specific

(B) Expression changes of unique genes in PC9DTPs compared with parental (par) PC9 cells treated with 1 μM erl for 24 hr. The RNA-seq analysis is based on three independent experiments normalized to an ERCC spike-in control (added based on cell number).
(C) The bargraph shows a few examples from the RNA-seq analysis of increased expression of IFN response/antiviral defense genes in the PC9DTPs compared with the parental population (logFC).
(D) qRT-PCR validation of increased expression of IFIH1, IRF7, OASL and RIG-1/DDX58 in PC9DTPs compared with PC9 cells. Relative changes in mRNA levels in PC9DTPs (black bars) compared with the parental population (gray bars). Ct values for each gene product were normalized using β-actin as the internal control.
(E) qRT-PCR analysis of IFIH1, IRF7, and RIG-1/DDX58 in ALDH^{high} cell populations with or without erl (12 hr). Ct values were normalized to β-actin.
(F and G) Heatmaps showing the ATAC-seq signal intensity in promoter regions (defined as −5 and +1 kb of the TSS) of the 21 IFN-related genes shown in the RNA-seq analysis in Figure 4C in PC9 and PC9DTP (F) or in ALDH^{low}, ALDH^{high}, ALDH^{low} + erl, and ALDH^{high} + erl FACS-sorted PC9 populations (G).
(H) Log_2 ratios showing ATAC-seq fragment length in PC9DTPs compared with parental PC9 cells. An average of three replicates is shown.
(I) Log_2 ratios showing the effect on ATAC-seq fragment lengths following erl treatment (1 μM, 12 hr) in FACS-sorted subpopulations of PC9 cells: ALDH^{High} (green) and ALDH^{low} (blue).
Error bars in (D and E) represent ±SD, which was calculated based on differences from three independent experiments in triplicate, and p values were generated using paired t test.
*p < 0.05, **p < 0.01, ***p < 0.001, ****p < 0.0001. See also Figure S4 and Tables S5 and S6.

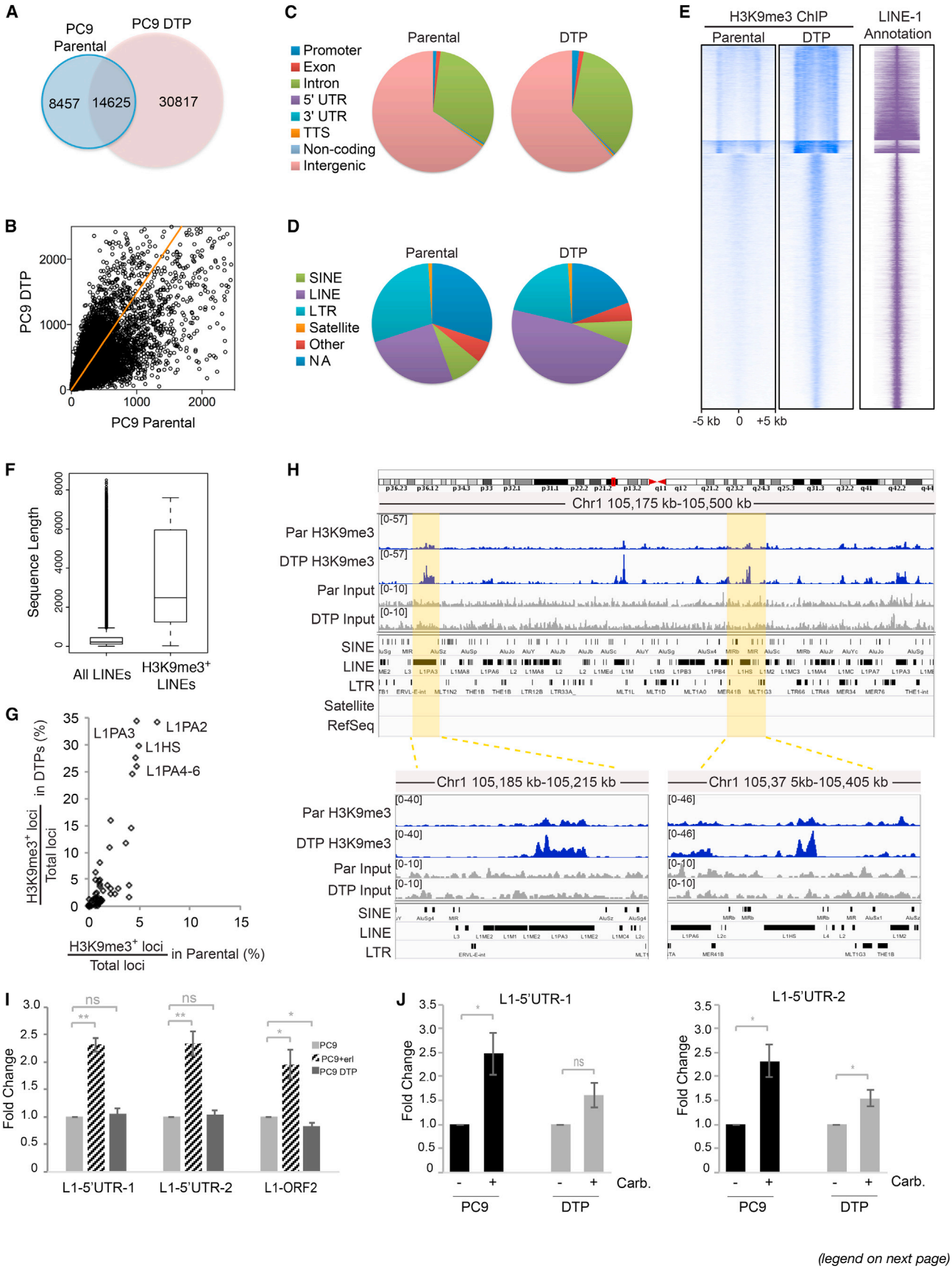

(legend on next page)

family L1HS (Lee et al., 2007; Ovchinnikov et al., 2002). By calculating the percent of LINE-1 loci covered by H3K9me3 compared with the total loci, we determined that the H3K9me3 enrichment in DTPs was most prominent over the primate-specific LINE-1s (Figures 5G and 5H). These findings raise the possibility that H3K9me3-mediated heterochromatin formation over LINE-1s prevents drug/stress-induced expression of such elements in DTPs.

Reduced Drug-Induced Expression of LINE-1 Elements in DTPs

The expression of transposable elements (TEs) such as LINE-1s can be induced by various stresses and we found that carboplatin (carb) and erl induce expression of repeat elements in PC9 cells (Table S6). Furthermore, an ATAC-seq analysis of TEs also showed more reads in erl-treated PC9 cells (Figure S5F). To investigate whether the increase in H3K9me3 over LINE-1s in DTPs corresponded to a decrease in their expression, we utilized a qRT-PCR approach using primers mapping to relatively conserved parts of LINE-1 transcripts. These studies revealed an increase in LINE-1 transcription following erl exposure in the bulk PC9 population, whereas PC9DTPs displayed expression levels similar to those observed in PC9 cells (Figure 5I). Furthermore, erl-generated PC9DTPs displayed a reduced induction of LINE-1 transcription following exposure to carboplatin (Figure 5J). These data, and an ATAC-seq analysis that shows a reduction in LINE-1 reads in PC9DTPs (Figures S5F and S5G), suggest that H3K9me3-mediated heterochromatin formation over LINE-1s contribute to DTP survival.

HDAC Inhibition De-represses LINE-1 Elements Specifically in DTPs

To verify that repression of LINE-1s contributes to DTP survival, we utilized an HDAC inhibitor to reverse the heterochromatin state, since studies have shown that HDAC activity is required for the maintenance of H3K9me3-mediated heterochromatin (Aygun et al., 2013). Our studies also showed that DTP populations display increased sensitivity to HDAC inhibitors TSA (Sharma et al., 2010) and MS275/entinostat *in vitro* (Figure S6A) and *in vivo* since erl-regressed PC9 tumors relapsed at a reduced rate when treated with the HDAC inhibitor MS275 (Figures 6A and S6B) or TSA (Figures S6C and S6D).

To establish a direct link between TSA-induced DTP death and reversal of H3K9me3-mediated heterochromatin formation over LINE-1s, we first investigated whether the TSA-induced death was preceded by changes in chromatin and/or expression of LINE-1s in DTPs. Apoptosis in DTPs occurs after only a few hours of exposure to low concentrations of TSA (Figure 6B); therefore, cells for these experiments were harvested 5–6 hr after treatment with TSA. A histone MS analysis following TSA exposure showed more extensive global H3PTM changes in PC9DTPs than in PC9s (Tables S1 and S4). For example, these experiments showed a DTP-specific increase in H3K14Ac on H3K9me3-containing peptides in PC9DTPs, suggesting a less compacted chromatin state over H3K9-methylated regions (Figure S6E). These data also showed a largely DTP-specific increase in H3K4me3 in response to TSA (Tables S1 and S4). Moreover, an ATAC-seq analysis of fragment length distribution in DTPs treated with TSA compared with DTPs also showed a decrease in longer fragments after TSA exposure, indicating a more open chromatin structure (Figure S6F, red line). To evaluate whether the TSA-induced changes in DTP chromatin could be seen over LINE-1s, we analyzed H3K9me3 and H3K4me3 ChIP-seq as well as ATAC-seq data from DTPs and DTPs treated with TSA. The analyzed data were organized in a strand-aware (5′-3′) manner over LINE-1s occupied by H3K9me3 and showed a slight decrease in H3K9me3 reads over full-length LINE-1s in TSA-treated DTPs (Figures 6C, 6D, and S6G). Furthermore, the analysis of the H3K4me3 ChIP-seq reads showed an increase in H3K4me3 in the 5′ UTR region of full-length LINE-1s in DTPs treated with TSA (Figures 6C, 6D, and S6G). A similar pattern was seen in the ATAC-seq data, which revealed an increase in transposase accessibility in the 5′ UTR of LINE-1s in TSA-treated DTPs (Figures 6C, 6D, S6G, and S6H).

Next, we investigated whether transcription of LINE-1s was induced in PC9DTPs treated with TSA. First, an analysis of

Figure 5. H3K9me3 Accumulates over LINE-1 Elements in PC9DTPs

(A) Venn diagram showing overlap among H3K9me3 ChIP-seq peaks identified in PC9 (23,082 peaks total) and PC9DTPs (45,422 peaks total).

(B) Scatterplot depicting the number of reads under H3K9me3 ChIP-seq peaks in the PC9 compared with PC9DTPs (n = 54,751 regions total, determined from a union of peaks in PC9 and DTPs).

(C and D) Distribution of H3K9me3 ChIP-seq peaks observed in PC9 parental cells and PC9DTPs over annotated gene (C) or repeat (D) features.

(E) Heatmaps showing LINE-1 annotation (purple) and H3K9me3 signal intensities (blue) in chromatin from PC9 or PC9DTPs over 10 kb windows centered around each of 22,399 LINE-1 elements that show H3K9me3 enrichment in PC9 and/or PC9DTPs.

(F) Boxplots showing the sequence-length distribution of all LINE-1 elements and H3K9me3-occupied LINE-1 elements (22,399 total) from the PC9 and/or PC9DTP datasets. The horizontal line inside the box represents median (50% percentile), and the lower and upper borders of the box correspond to 25th and 75th percentiles, respectively. H-spread, 1.5×, showing variability is depicted by whiskers of the boxplot and the data points beyond the limit of whiskers denote outliers.

(G) Percentage of total copies with a H3K9me3 ChIP-seq peak for LINE-1 sequences in chromatin from PC9 parental cells (x axis) and PC9DTPs (y axis). L1PA2-6 and L1Hs represent primate-specific LINE-1s.

(H) Two examples of genomic regions with LINE-1 elements that exhibit increased H3K9me3 ChIP-seq signal in chromatin from PC9DTPs compared with PC9. Input signal (different scale) and annotation are shown at the bottom of the panels.

(I) qRT-PCR analysis of LINE-1 expression, using several sets of primers to conserved LINE-1 regions, in drug-naive (PC9) or erl-treated (PC9 + erl, 1 μM for 15 hr) and PC9DTPs. The analysis was performed using data from three independent experiments run in triplicate normalized to β-actin.

(J) qRT-PCR analysis in PC9 and PC9DTPs exposed to carboplatin (carb, 50 μM for 3 days), using two primer sets to conserved LINE-1 regions. The analysis was performed using data from three independent experiments in triplicate normalized to β-actin.

Error bars in (I and J) represent ±SD, which was calculated based on the fold change in the three experiments in triplicate and p values were calculated using paired t test.

ns > 0.05, *p < 0.05, **p < 0.01. See also Figure S5.

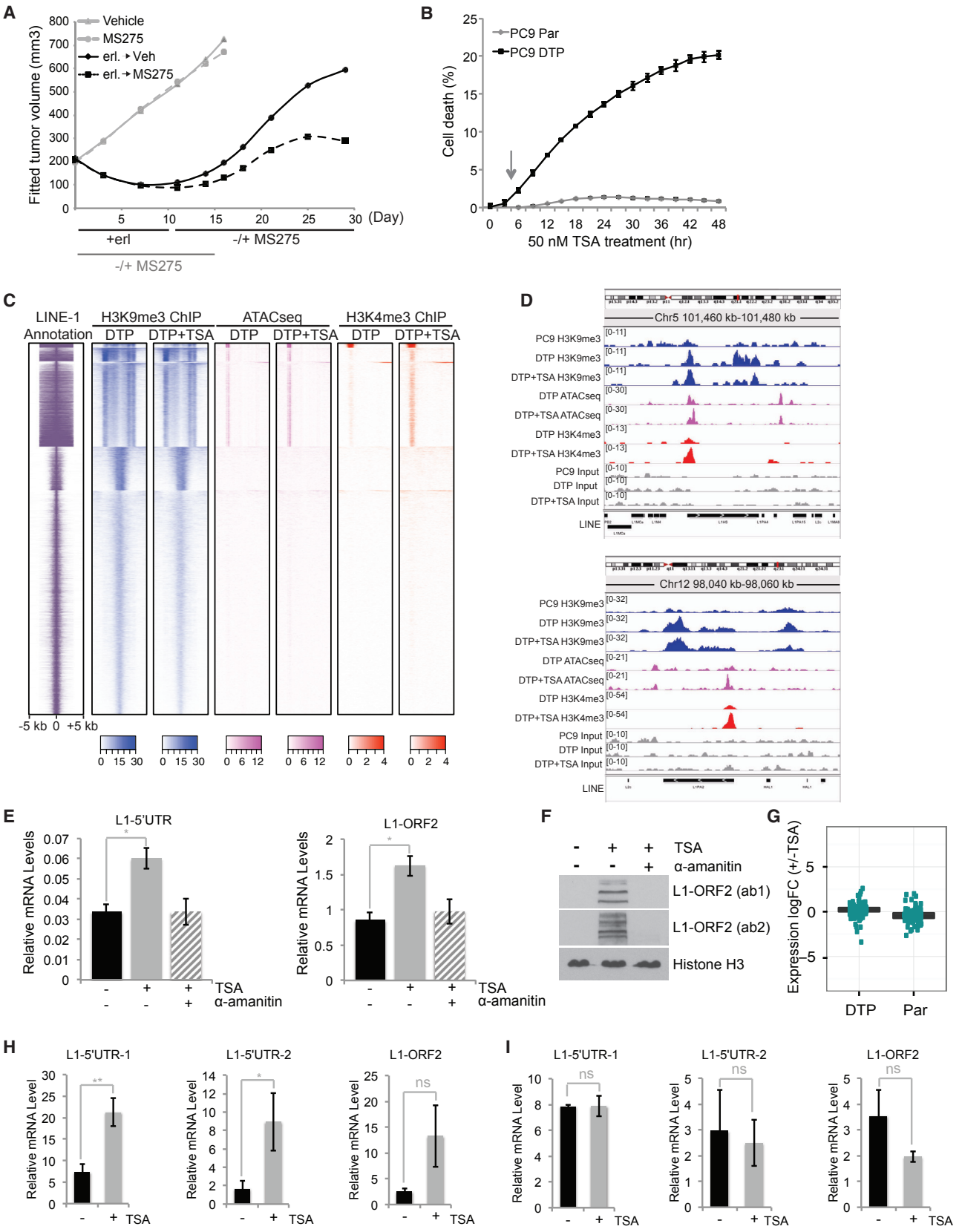

(legend on next page)

qRT-PCR data demonstrated that short-term TSA exposure resulted in increased LINE-1 transcription in DTPs that was blocked by the RNA polymerase inhibitor α-amanitin (Figure 6E). The TSA-induced LINE-1 expression was also confirmed using antibodies that recognize the LINE-1 ORF2 protein (Figure 6F). To determine whether the TSA-induced changes in LINE-1 transcription were unique to DTPs we analyzed their expression in the RNA-seq data from parental and DTP samples treated with TSA. This analysis demonstrated a slight decrease in LINE-1 transcription in response to TSA in the parental population, whereas LINE-1 transcription was somewhat induced in DTPs treated with TSA (Figures 6G and S6I; Table S7). We also examined the expression changes in other repeat families in PC9 and PC9DTPs treated with TSA (Table S7). To verify these findings, we also assessed expression of LINE-1s in PC9 and DTP populations treated with TSA by qRT-PCR. This analysis included normalization to β-actin expression as well as to one of the spike-in control RNAs (Figures 6H, 6I, and S6J), and showed a general increase in LINE-1 transcription in DTPs treated with TSA. Collectively, these findings suggest that low doses of TSA disrupt the H3K9me3-mediated heterochromatin state over LINE-1s and result in induction of their expression in the DTP population.

TSA-Induced LINE-1 Expression Contributes to the Ablation of the DTP Population

Repression of LINE-1s in DTPs could create a counterbalance to the drug-induced expression of repeat RNA sequences and IFN response/antiviral defense genes. Consistent with this hypothesis, KD of the viral sensor Rig-1/DDX58 resulted in a partial rescue of the TSA-induced ablation of the DTP population (Figure 7A). Rig-1/DDX58-depleted cells did not show a significant increase in the number of parental cells or cells that survive erl exposure compared with the non-targeting control (Figure S7A). Next, to establish a direct relationship between TSA-induced LINE-1 transcription and the adverse effect of TSA on DTP survival, we used siRNAs targeting conserved regions of evolutionarily young LINE-1s (Aschacher et al., 2016). These siRNAs reduced LINE-1 expression in transfected PC9 cells (Figure 7B). The LINE-1 siRNAs did not significantly affect the survival of the bulk population following erl treatment, but they partially rescued the reduced number of PC9DTPs seen upon TSA treatment (Figure 7C).

In addition to a general increase in repeat RNA expression (Table S7), the TSA-induced expression of the LINE-1 ORF2-encoded reverse transcriptase could contribute to reduced genomic fitness by promoting retro-transposition of LINE-1s as well as that of non-autonomous TEs such as SINE-1s, which could result in damage to DTP genomes. Therefore, to further analyze whether repression of LINE-1 function is important for DTP survival, we used pharmacologic inhibitors (reverse transcriptase inhibitors [RT-i], zidovudine, and didanosine) that interfere with the reverse transcriptase function of L1-ORF2 (Dai et al., 2011). First, PC9 cells were treated with the RT-i in combination with erl, or erl and TSA, for 3 days. Consistent with previous observations (Sciamanna et al., 2005), the RT-i caused mild cytotoxicity in PC9 cells in the absence or presence of TSA (Figure S7B) and negatively affected their survival in erl (Figures 7D and 7E). In sharp contrast, the TSA-induced reduction in DTPs was partially rescued by the RT-i (Figures 7D and 7E). The partial rescue of the TSA-induced ablation of DTPs by the RT-i was also observed when established DTPs (day 4) were treated with TSA, in marked contrast to the cytotoxic effect displayed by the RT-i alone on established DTPs (Figures 7F, 7G, S7C, and S7D). Importantly, the decreased number of DTPs seen in response to a reduction in H3K27me3, which did not accumulate over LINE-1s in DTPs (data not shown), was not rescued by the RT-i (Figure S7E). Together, these results demonstrate that increased expression of LINE-1s contributes to the TSA-induced ablation of the DTP population (Figure 7H).

DISCUSSION

Collectively, our findings suggest that epigenetic repression of TEs, including H3K9me3-mediated repression of LINE-1s, is a mechanism by which a subpopulation of cancer cells transiently survive otherwise lethal drug exposures. In the context of evolution, activation, and propagation of TEs enables organisms to

Figure 6. HDAC Inhibitors Increase Expression of LINE-1s and Cause Cell Death Selectively in the DTP Population

(A) Tumor growth curves in mice with established PC9 xenograft tumors treated with erl, MS275, or erl, followed by MS275. Tumor growth curves are presented as linear mixed effects fit analysis of tumor volume graphed as cubic splines with auto-determined knots.

(B) PC9 cells (gray) and PC9DTPs (black) treated with 50 nM TSA followed by IncuCyteZoom quantification of cell death using a reagent that detects caspase-3 cleavage. A representative experiment performed in triplicate is shown.

(C) Heatmaps showing H3K9me3 ChIP-seq (blue), ATAC-seq (magenta), or H3K4me3 ChIP-seq signals (red) over all H3K9me3 ChIP-seq peaks that map to 22,399 LINE-1s in chromatin from PC9 and/or PC9DTPs. Clusters were generated in a "strand-aware" manner to orient LINE-1s on different DNA strands in the same direction. Data from DTPs or TSA-treated DTPs are shown.

(D) Genome browser views for two example regions with increased H3K9me3 (blue) in DTPs over an evolutionarily young LINE-1; ATAC-seq (magenta) and H3K4me3 (red).

(E and F) TSA-induced increases in LINE-1 RNA as measured by SYBR green qRT-PCR using three probes (E) and LINE-1 ORF2 protein levels (F) in PC9DTPs treated with 50 nM TSA for 3 hr in the presence or absence of α-amanitin (1 μg/mL, RNA polymerase inhibitor).

(G) RNA-seq analysis of TSA-induced LINE-1 expression changes in PC9 and PC9DTP populations. The analysis is based on three independent experiments using an ERCC spike-in control to normalize the data (added based on cell number). Boxplots showing the logFC when TSA-treated PC9 and PC9DTPs are compared with control treated cells. The line inside the box represents median (50% percentile), and the lower and upper borders of the box correspond to 25th and 75th percentiles, respectively (boxplots look like lines due to low variance). The turquoise dots represent LINE-1s that show a change in expression.

(H and I) TSA-induced LINE-1 expression in PC9DTPs (H) and PC9 parental (I) by qRT-PCR analysis using probes against various LINE-1 element regions as indicated.

The error bars in (E, H, and I) represent ± SD, which was calculated based on three separate experiments in triplicate where the Ct values were normalized to β-actin, and p values were calculated using unpaired t test.

ns > 0.05, *p < 0.05, **p < 0.01. See also Figure S6 and Table S7.

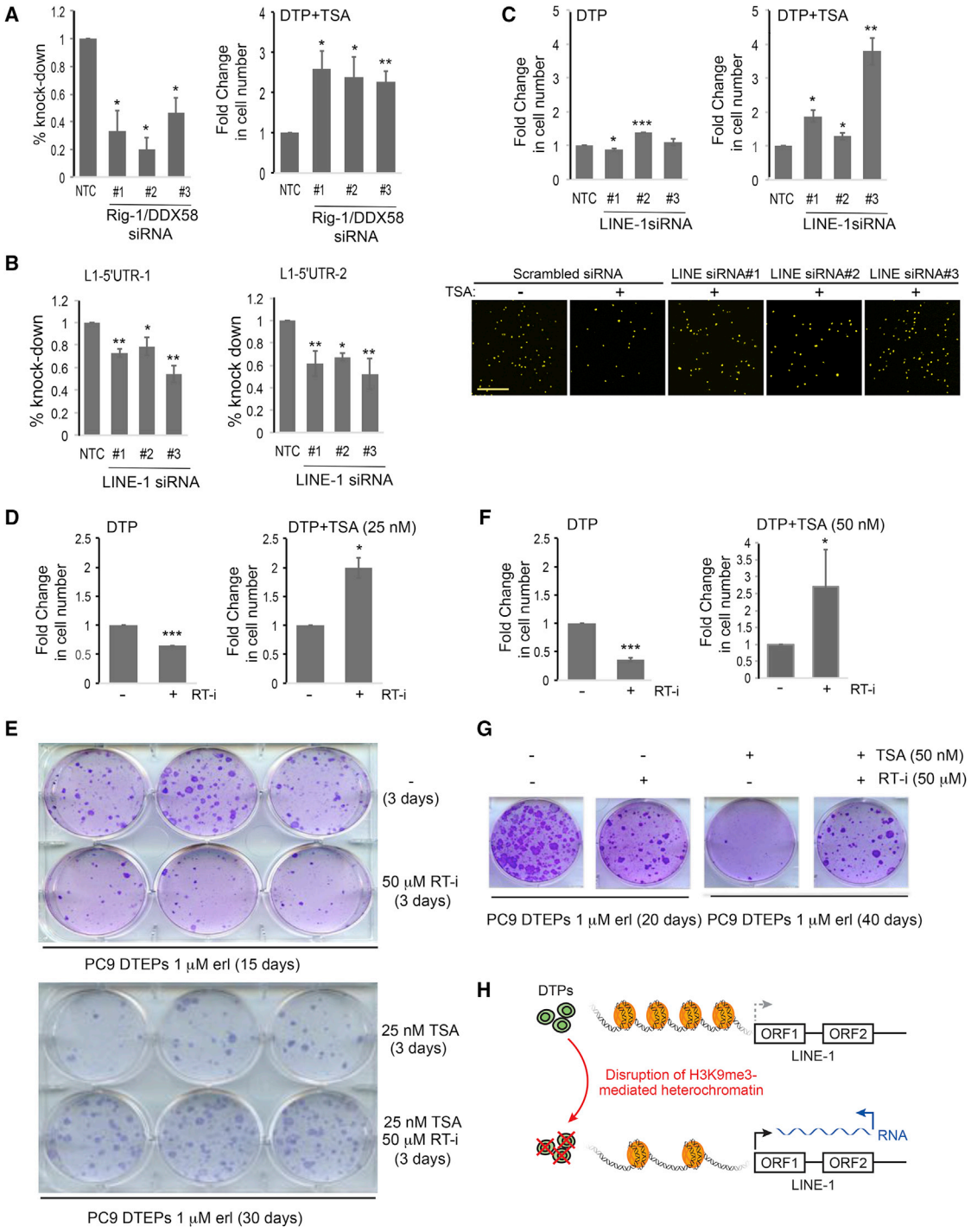

Figure 7. HDAC Inhibitor-Induced Death in DTPs Is Partially Rescued by Reduced LINE-1 Element Expression/Function

(A) Efficiencies of Rig-1/DDX58 KD (left) and the effect of Rig-1/DDX58 KD on TSA-induced death in PC9 (right) for three individual Rig-1/DDX58 siRNAs compared with the NTC control. The percentage of KD was normalized to β-actin, based on two independent experiments in triplicate, ±SD was calculated based on the differences in the percentage of KD compared with the NTC, and p values were calculated using paired t test.

(B) KD efficiencies of LINE-1 siRNAs numbers 1–3 compared with the NTC. The analysis is based on three independent experiments in triplicate. Shown are an average of ratios of the three experiments, error bars represent the ±SD of the percentage of KD compared with the NTC, and p values were calculated with paired t test.

(C) Effect of LINE-1 KD on TSA-induced DTP death as determined by the number of DTPs that survive 6-day erl treatment in the presence or absence of 25 nM TSA. The IncuCyteZoom analysis is presented as the average fold change for each siRNA compared with the NTC. Error bars represent ±SD from two

(legend continued on next page)

adapt to changing conditions by generating genomic diversity (McClintock, 1984; Mourier et al., 2014), but can also result in reduced fitness. Consequently, organisms have developed elaborate mechanisms to control their activation (Gifford et al., 2013). In the context of heterogeneous cancer cell drug responses, activation of TEs could provide adaptation benefits during drug exposure, but their activation could also undermine cancer cell fitness. Therefore, the epigenetic repression of TEs may provide a drug-tolerant population with a reversible genome-protective mechanism that ensures cell survival during lethal drug exposures. Interestingly, it has previously been shown that proteins involved in H3K9me3-mediated heterochromatin formation can serve as guardians of genomic integrity, by reducing TE activation during stages of development in which these regions are transiently DNA hypomethylated (Liu et al., 2014; Matsui et al., 2010).

In contrast to the mostly repressed and DNA-methylated state of TEs in differentiated tissues, cancer cells display DNA hypomethylation in regions containing TEs (Feinberg and Vogelstein, 1987), suggesting increased expression and activity of these elements in tumors. In fact, it has been suggested that hypomethylation of TEs correlates with genome instability in NSCLC (Iskow et al., 2010). Other studies have implicated LINE-1 transposition in tumor development (Doucet-O'Hare et al., 2015; Ewing et al., 2015; Rodic et al., 2015). Recent studies have also suggested that expression of TEs has an impact on the effectiveness of tumor immunotherapy (Chiappinelli et al., 2015; Rooney et al., 2015; Roulois et al., 2015). In this context, it is interesting to note that our studies show that cancer drugs such as carboplatin can induce the expression of TEs, and recent clinical trials have shown that carboplatin can enhance the response to anti-PD1. Furthermore, drug-induced activation of TEs and antiviral proteins such as APOBEC3A may contribute to the genetic alterations that have been found in patients that have relapsed on cancer drugs.

Our studies suggest that HDAC and other epigenetic inhibitors that prevent the establishment of a heterochromatic state in the "dormant" DTP population results in reduced DTP numbers, and we note that DNA demethylating agents as well as HDAC inhibitors have shown promise in early clinical studies in relapsed cancer patients. However, considering that acquired drug resistance may involve multiple diverse molecular mechanisms within the same patient, future studies will certainly be required to establish the clinical utility of a therapeutic strategy that involves disruption of the heterochromatin state in DTPs. In summary, the observations presented here suggest that DTPs deploy a developmental mechanism that promotes silencing of TEs to protect the integrity of their genomes in response to potentially lethal stress. A similar population survival strategy appears to be well conserved throughout evolution, although distinct mechanisms may be involved.

STAR★METHODS

Detailed methods are provided in the online version of this paper and include the following:

- KEY RESOURCES TABLE
- CONTACT FOR REAGENT AND RESOURCE SHARING
- EXPERIMENTAL MODEL AND SUBJECT DETAILS
  - Cell Lines and Genomic Annotations
  - Cell Culture Conditions
  - Mouse Xenograft Experiments
  - Patient Samples
- METHOD DETAILS
  - Inhibitors Used
  - DTP Generation
  - Immunoblotting
  - Immunofluorescence and Immunohistochemistry Using Xenograft Tumor Material
  - Aldefluor Staining
  - Epigenetic Inhibitor Cell Assays
  - Xenograft Studies
  - Reverse Transcriptase Inhibitor Studies
  - Caspase-3/7 Cleavage Assay
  - siRNA Screen
  - siRNA Knock-Down of LINE-1 elements and Rig-1/DDX58
  - CRISPR-mediated Gene Targeting of *G9a/EHMT2/KMT1C*, *EZH2* and *H3F3B*
  - Inducible shRNA Knock-down of SETDB1
  - Subcellular Fractionation
  - Salt Fractionation
  - RNA Analysis by qRT-PCR of Parental and DTP Cells
  - Sample Generation for RNA Studies
  - LINE-1 RNA Analysis by Taqman
  - LINE-1 RNA Analysis by SYBR Green qRT-PCR
  - Taqman Analysis of IFN Response/Antiviral Defense Genes

independent experiments in triplicate, and p values were calculated using paired t test. Representative images as indicated are shown in the bottom panels (cells pseudo-colored yellow). Scale bar, 800 μm.

(D) PC9 cells were plated in erl in the absence or presence of 50 μM zidovudine and didanosine (RT-i) in the absence or presence of 25 nM TSA as indicated. The IncuCyteZoom analysis represents the average fold change from three independent experiments in triplicate, error bars represent the ±SD in the fold change, and p values were calculated based using paired t test.

(E) Transition of DTPs to DTEPs in erl following a 3-day exposure to erl (–/+ TSA) and –/+ RT-I (DTEP, 15 days for erl –/+ RT-i plate, top panel, and 30 days for erl + TSA –/+ RT-i plate, bottom panel). A Giemsa-stained representative 6-well plate is shown in each case.

(F) The data are presented as fold change in the number of day 4 erl-derived PC9DTPs treated with RT-i or TSA and –/+ RT-i for an additional 3 days. Cell numbers were determined using IncuCyteZoom imaging and error bars represent ±SD in the fold change between the three independent experiments in triplicate, and p values were calculated using paired t test.

(G) Outgrowth of PC9DTPs to DTEPs in erl (DTEP, 20 or 40 days) after day 4 DTPs were exposed to the indicated drugs for 3 days.

(H) Model depicting the proposed role of H3K9me3-mediated heterochromatin repression of drug-induced LINE-1 transcription in promoting survival of DTPs. Disruption of the H3K9me3-mediated heterochromatin state in PC9DTPs by TSA treatment increases LINE-1 expression, which contributes to the ablation of the DTP population.

*p < 0.05, **p < 0.01, ***p < 0.001. See also Figure S7.

SUPPLEMENTAL INFORMATION

Supplemental Information includes seven figures and seven tables and can be found with this article online at http://dx.doi.org/10.1016/j.ccell.2017.07.002.

AUTHOR CONTRIBUTIONS

C.A.T., G.D.G., C.W., M.C., and R.P. performed most of the experiments presented. H.-J.K. performed *in vitro* epigenetic inhibitor experiments, K.N. and J.-P.S. performed and analyzed the siRNA screen, T.K.C. and D.A. were responsible for histone MS experiments and analysis, M.W. and Y.Y. provided patient data, B.H. and T.C. provided vectors for short hairpin KD and CRISPR guide RNA design, J.W. provided IHC analysis support, N.A., G.H., and E.J. ran xenograft experiments, J.L. and S.J. performed the RNA-seq analysis, K.-B.C., T.L.N., P.G.G., and G.D.G. performed the ATAC-seq analysis, G.D.G. performed the H3K9me3 and H3K4me3 ChIP-seq analysis. M.C. oversaw all experiments and wrote the paper with help from C.A.T., G.D.G., R.P., J.S., C.W., S.J., K.-B.C., T.L.N., and D.A.

ACKNOWLEDGMENTS

We thank K. Finn, M. Costa, and T. Lau for DTP generation in the GTL-16 and SW480 models, M. Craske, P. Labhart, and B. Egan at Active Motif for ChIP-seq and ATAC-seq, S. Memarsadeghi at Essenbiosciences for optimization of DTP detection, and A. Bruce for illustration help. We also would like to thank the Genentech FACS facility for excellent technical support, D. Dunlap, K. Mesh, and J. Hung for IHC support, P. Polakis, H. Phillips, A. Cochran, L. Yamasaki, P. Trojer, and K. LaMarco for valuable suggestions throughout the course of this work, and to the inspiration that G. Klein provided to M.C. C.W., T.K.C., M.W., Y.Y., B.H., S.J., J.W., and D.A. are all employees of Genentech Inc. and may hold Roche stock, J.-P. S. is employed by Servier, P.G.G. and T.L.N. are employed by Epinomics, and K.-B.C. is employed by Active Motif and may hold stock, G.D.G. is employed by Celgene Corporation and may hold stock, J.L. is employed by Gilead and may hold stock, C.A.T. is employed by Clara Foods, E.J. and G.H. are employed by ORIC Pharmaceuticals, and J.S. is an employee of Calico Life Sciences Inc.

Received: August 24, 2016
Revised: May 2, 2017
Accepted: July 5, 2017
Published: August 3, 2017

REFERENCES

Allis, C.D., and Jenuwein, T. (2016). The molecular hallmarks of epigenetic control. Nat. Rev. Genet. *17*, 487–500.

Aschacher, T., Wolf, B., Enzmann, F., Kienzl, P., Messner, B., Sampl, S., Svoboda, M., Mechtcheriakova, D., Holzmann, K., and Bergmann, M. (2016). LINE-1 induces hTERT and ensures telomere maintenance in tumour cell lines. Oncogene *35*, 94–104.

Aygun, O., Mehta, S., and Grewal, S.I. (2013). HDAC-mediated suppression of histone turnover promotes epigenetic stability of heterochromatin. Nat. Struct. Mol. Biol. *20*, 547–554.

Balaban, N.Q., Gerdes, K., Lewis, K., and McKinney, J.D. (2013). A problem of persistence: still more questions than answers? Nat. Rev. Microbiol. *11*, 587–591.

Barski, A., Cuddapah, S., Cui, K., Roh, T.Y., Schones, D.E., Wang, Z., Wei, G., Chepelev, I., and Zhao, K. (2007). High-resolution profiling of histone methylations in the human genome. Cell *129*, 823–837.

Buenrostro, J.D., Giresi, P.G., Zaba, L.C., Chang, H.Y., and Greenleaf, W.J. (2013). Transposition of native chromatin for fast and sensitive epigenomic profiling of open chromatin, DNA-binding proteins and nucleosome position. Nat. Methods *10*, 1213–1218.

Buenrostro, J.D., Wu, B., Chang, H.Y., and Greenleaf, W.J. (2015). ATAC-seq: a method for assaying chromatin accessibility genome-wide. Curr. Protoc. Mol. Biol. *109*, 21.29.1–21.29.9.

Cantone, I., and Fisher, A.G. (2013). Epigenetic programming and reprogramming during development. Nat. Struct. Mol. Biol. *20*, 282–289.

Chen, L., Dahlstrom, J.E., Lee, S.H., and Rangasamy, D. (2012). Naturally occurring endo-siRNA silences LINE-1 retrotransposons in human cells through DNA methylation. Epigenetics *7*, 758–771.

Chiappinelli, K.B., Strissel, P.L., Desrichard, A., Li, H., Henke, C., Akman, B., Hein, A., Rote, N.S., Cope, L.M., Snyder, A., et al. (2015). Inhibiting DNA methylation causes an interferon response in cancer via dsRNA including endogenous retroviruses. Cell *162*, 974–986.

Cong, L., Ran, F.A., Cox, D., Lin, S., Barretto, R., Habib, N., Hsu, P.D., Wu, X., Jiang, W., Marraffini, L.A., et al. (2013). Multiplex genome engineering using CRISPR/Cas systems. Science *339*, 819–823.

Coufal, N.G., Garcia-Perez, J.L., Peng, G.E., Yeo, G.W., Mu, Y., Lovci, M.T., Morell, M., O'Shea, K.S., Moran, J.V., and Gage, F.H. (2009). L1 retrotransposition in human neural progenitor cells. Nature *460*, 1127–1131.

Dai, L., Huang, Q., and Boeke, J.D. (2011). Effect of reverse transcriptase inhibitors on LINE-1 and Ty1 reverse transcriptase activities and on LINE-1 retrotransposition. BMC Biochem. *12*, 18.

Darmon, E., and Leach, D.R. (2014). Bacterial genome instability. Microbiol. Mol. Biol. Rev. *78*, 1–39.

de Jong, I.G., Haccou, P., and Kuipers, O.P. (2011). Bet hedging or not? A guide to proper classification of microbial survival strategies. Bioessays *33*, 215–223.

Doucet-O'Hare, T.T., Rodic, N., Sharma, R., Darbari, I., Abril, G., Choi, J.A., Young Ahn, J., Cheng, Y., Anders, R.A., Burns, K.H., et al. (2015). LINE-1 expression and retrotransposition in Barrett's esophagus and esophageal carcinoma. Proc. Natl. Acad. Sci. USA *112*, E4894–E4900.

Ewing, A.D., Gacita, A., Wood, L.D., Ma, F., Xing, D., Kim, M.S., Manda, S.S., Abril, G., Pereira, G., Makohon-Moore, A., et al. (2015). Widespread somatic L1 retrotransposition occurs early during gastrointestinal cancer evolution. Genome Res. *25*, 1536–1545.

Feil, R., and Fraga, M.F. (2011). Epigenetics and the environment: emerging patterns and implications. Nat. Rev. Genet. *13*, 97–109.

Feinberg, A.P., and Vogelstein, B. (1987). Alterations in DNA methylation in human colon neoplasia. Semin. Surg. Oncol. *3*, 149–151.

Filipescu, D., Muller, S., and Almouzni, G. (2014). Histone H3 variants and their chaperones during development and disease: contributing to epigenetic control. Annu. Rev. Cell Dev. Biol. *30*, 615–646.

Gal-Yam, E.N., Egger, G., Iniguez, L., Holster, H., Einarsson, S., Zhang, X., Lin, J.C., Liang, G., Jones, P.A., and Tanay, A. (2008). Frequent switching of Polycomb repressive marks and DNA hypermethylation in the PC3 prostate cancer cell line. Proc. Natl. Acad. Sci. USA *105*, 12979–12984.

Gifford, W.D., Pfaff, S.L., and Macfarlan, T.S. (2013). Transposable elements as genetic regulatory substrates in early development. Trends Cell Biol *23*, 218–226.

Goodier, J.L., and Kazazian, H.H., Jr. (2008). Retrotransposons revisited: the restraint and rehabilitation of parasites. Cell *135*, 23–35.

Groenendijk, F.H., and Bernards, R. (2014). Drug resistance to targeted therapies: deja vu all over again. Mol. Oncol. *8*, 1067–1083.

Guo, H., Chitiprolu, M., Gagnon, D., Meng, L., Perez-Iratxeta, C., Lagace, D., and Gibbings, D. (2014). Autophagy supports genomic stability by degrading retrotransposon RNA. Nat. Commun. *5*, 5276.

Hancks, D.C., and Kazazian, H.H., Jr. (2012). Active human retrotransposons: variation and disease. Curr. Opin. Genet. Dev. *22*, 191–203.

Hata, A.N., Niederst, M.J., Archibald, H.L., Gomez-Caraballo, M., Siddiqui, F.M., Mulvey, H.E., Maruvka, Y.E., Ji, F., Bhang, H.E., Krishnamurthy Radhakrishna, V., et al. (2016). Tumor cells can follow distinct evolutionary paths to become resistant to epidermal growth factor receptor inhibition. Nat. Med. *22*, 262–269.

Holden, D.W. (2015). Microbiology. Persisters unmasked. Science *347*, 30–32.

Iskow, R.C., McCabe, M.T., Mills, R.E., Torene, S., Pittard, W.S., Neuwald, A.F., Van Meir, E.G., Vertino, P.M., and Devine, S.E. (2010). Natural mutagenesis of human genomes by endogenous retrotransposons. Cell *141*, 1253–1261.

Iwase, S., Xiang, B., Ghosh, S., Ren, T., Lewis, P.W., Cochrane, J.C., Allis, C.D., Picketts, D.J., Patel, D.J., Li, H., et al. (2011). ATRX ADD domain links an atypical histone methylation recognition mechanism to human mental-retardation syndrome. Nat. Struct. Mol. Biol. *18*, 769–776.

Jinek, M., East, A., Cheng, A., Lin, S., Ma, E., and Doudna, J. (2013). RNA-programmed genome editing in human cells. Elife *2*, e00471.

Karolchik, D., Hinrichs, A.S., Furey, T.S., Roskin, K.M., Sugnet, C.W., Haussler, D., and Kent, W.J. (2004). The UCSC Table Browser data retrieval tool. Nucleic Acids Res. *32*, D493–D496.

Kattar, S.D., Surdi, L.M., Zabierek, A., Methot, J.L., Middleton, R.E., Hughes, B., Szewczak, A.A., Dahlberg, W.K., Kral, A.M., Ozerova, N., et al. (2009). Parallel medicinal chemistry approaches to selective HDAC1/HDAC2 inhibitor (SHI-1:2) optimization. Bioorg. Med. Chem. Lett. *19*, 1168–1172.

Kent, W.J., Zweig, A.S., Barber, G., Hinrichs, A.S., and Karolchik, D. (2010). BigWig and BigBed: enabling browsing of large distributed datasets. Bioinformatics *26*, 2204–2207.

Knoechel, B., Roderick, J.E., Williamson, K.E., Zhu, J., Lohr, J.G., Cotton, M.J., Gillespie, S.M., Fernandez, D., Ku, M., Wang, H., et al. (2014). An epigenetic mechanism of resistance to targeted therapy in T cell acute lymphoblastic leukemia. Nat. Genet. *46*, 364–370.

Kuczynski, E.A., Sargent, D.J., Grothey, A., and Kerbel, R.S. (2013). Drug rechallenge and treatment beyond progression – implications for drug resistance. Nat. Rev. Clin. Oncol. *10*, 571–587.

Kumar, P., Goh, G., Wongphayak, S., Moreau, D., and Bard, F. (2013). ScreenSifter: analysis and visualization of RNAi screening data. BMC Bioinformatics *14*, 290.

Langmead, B., Trapnell, C., Pop, M., and Salzberg, S.L. (2009). Ultrafast and memory-efficient alignment of short DNA sequences to the human genome. Genome Biol. *10*, R25.

Law, C.W., Chen, Y., Shi, W., and Smyth, G.K. (2014). voom: precision weights unlock linear model analysis tools for RNA-seq read counts. Genome Biol. *15*, R29.

Lee, J., Cordaux, R., Han, K., Wang, J., Hedges, D.J., Liang, P., and Batzer, M.A. (2007). Different evolutionary fates of recently integrated human and chimpanzee LINE-1 retrotransposons. Gene *390*, 18–27.

Li, H., and Durbin, R. (2010). Fast and accurate long-read alignment with Burrows-Wheeler transform. Bioinformatics *26*, 589–595.

Liu, S., Brind'Amour, J., Karimi, M.M., Shirane, K., Bogutz, A., Lefebvre, L., Sasaki, H., Shinkai, Y., and Lorincz, M.C. (2014). Setdb1 is required for germline development and silencing of H3K9me3-marked endogenous retroviruses in primordial germ cells. Genes Dev. *28*, 2041–2055.

MacLean, B., Tomazela, D.M., Shulman, N., Chambers, M., Finney, G.L., Frewen, B., Kern, R., Tabb, D.L., Liebler, D.C., and MacCoss, M.J. (2010). Skyline: an open source document editor for creating and analyzing targeted proteomics experiments. Bioinformatics *26*, 966–968.

Maile, T.M., Izrael-Tomasevic, A., Cheung, T., Guler, G.D., Tindell, C., Masselot, A., Liang, J., Zhao, F., Trojer, P., Classon, M., et al. (2015). Mass spectrometric quantification of histone post-translational modifications by a hybrid chemical labeling method. Mol. Cell Proteomics *14*, 1148–1158.

Mali, P., Yang, L., Esvelt, K.M., Aach, J., Guell, M., DiCarlo, J.E., Norville, J.E., and Church, G.M. (2013). RNA-guided human genome engineering via Cas9. Science *339*, 823–826.

Matsui, T., Leung, D., Miyashita, H., Maksakova, I.A., Miyachi, H., Kimura, H., Tachibana, M., Lorincz, M.C., and Shinkai, Y. (2010). Proviral silencing in embryonic stem cells requires the histone methyltransferase ESET. Nature *464*, 927–931.

McArthur, G.A., Puzanov, I., Amaravadi, R., Ribas, A., Chapman, P., Kim, K.B., Sosman, J.A., Lee, R.J., Nolop, K., Flaherty, K.T., et al. (2012). Marked, homogeneous, and early [18F]fluorodeoxyglucose-positron emission tomography responses to vemurafenib in BRAF-mutant advanced melanoma. J. Clin. Oncol. *30*, 1628–1634.

McClintock, B. (1984). The significance of responses of the genome to challenge. Science *226*, 792–801.

Mendez, J., and Stillman, B. (2000). Chromatin association of human origin recognition complex, cdc6, and minichromosome maintenance proteins during the cell cycle: assembly of prereplication complexes in late mitosis. Mol. Cell. Biol. *20*, 8602–8612.

Mikkelsen, T.S., Ku, M., Jaffe, D.B., Issac, B., Lieberman, E., Giannoukos, G., Alvarez, P., Brockman, W., Kim, T.K., Koche, R.P., et al. (2007). Genome-wide maps of chromatin state in pluripotent and lineage-committed cells. Nature *448*, 553–560.

Mourier, T., Nielsen, L.P., Hansen, A.J., and Willerslev, E. (2014). Transposable elements in cancer as a by-product of stress-induced evolvability. Front. Genet. *5*, 156.

Noh, K.M., Allis, C.D., and Li, H. (2016). Reading between the Lines: "ADD"-ing histone and DNA methylation marks toward a new epigenetic "Sum". ACS Chem. Biol. *11*, 554–563.

Ovchinnikov, I., Rubin, A., and Swergold, G.D. (2002). Tracing the LINEs of human evolution. Proc. Natl. Acad. Sci. USA *99*, 10522–10527.

Patro, R., Duggal, G., Love, M.I., Irizarry, R.A., and Kingsford, C. (2017). Salmon provides fast and bias-aware quantification of transcript expression. Nat. Methods *14*, 417–419.

Raha, D., Wilson, T.R., Peng, J., Peterson, D., Yue, P., Evangelista, M., Wilson, C., Merchant, M., and Settleman, J. (2014). The cancer stem cell marker aldehyde dehydrogenase is required to maintain a drug-tolerant tumor cell subpopulation. Cancer Res. *74*, 3579–3590.

Rai, M., Soragni, E., Chou, C.J., Barnes, G., Jones, S., Rusche, J.R., Gottesfeld, J.M., and Pandolfo, M. (2010). Two new pimelic diphenylamide HDAC inhibitors induce sustained frataxin upregulation in cells from Friedreich's ataxia patients and in a mouse model. PLoS One *5*, e8825.

Ramirez, M., Rajaram, S., Steininger, R.J., Osipchuk, D., Roth, M.A., Morinishi, L.S., Evans, L., Ji, W., Hsu, C.H., Thurley, K., et al. (2016). Diverse drug-resistance mechanisms can emerge from drug-tolerant cancer persister cells. Nat. Commun. *7*, 10690.

Robinson, M.D., McCarthy, D.J., and Smyth, G.K. (2010). edgeR: a Bioconductor package for differential expression analysis of digital gene expression data. Bioinformatics *26*, 139–140.

Rodic, N., Steranka, J.P., Makohon-Moore, A., Moyer, A., Shen, P., Sharma, R., Kohutek, Z.A., Huang, C.R., Ahn, D., Mita, P., et al. (2015). Retrotransposon insertions in the clonal evolution of pancreatic ductal adenocarcinoma. Nat. Med. *21*, 1060–1064.

Roesch, A., Fukunaga-Kalabis, M., Schmidt, E.C., Zabierowski, S.E., Brafford, P.A., Vultur, A., Basu, D., Gimotty, P., Vogt, T., and Herlyn, M. (2010). A temporarily distinct subpopulation of slow-cycling melanoma cells is required for continuous tumor growth. Cell *141*, 583–594.

Rooney, M.S., Shukla, S.A., Wu, C.J., Getz, G., and Hacohen, N. (2015). Molecular and genetic properties of tumors associated with local immune cytolytic activity. Cell *160*, 48–61.

Roulois, D., Loo Yau, H., Singhania, R., Wang, Y., Danesh, A., Shen, S.Y., Han, H., Liang, G., Jones, P.A., Pugh, T.J., et al. (2015). DNA-demethylating agents

target colorectal cancer cells by inducing viral mimicry by endogenous transcripts. Cell *162*, 961–973.

Sciamanna, I., Landriscina, M., Pittoggi, C., Quirino, M., Mearelli, C., Beraldi, R., Mattei, E., Serafino, A., Cassano, A., Sinibaldi-Vallebona, P., et al. (2005). Inhibition of endogenous reverse transcriptase antagonizes human tumor growth. Oncogene *24*, 3923–3931.

Sharma, S.V., Lee, D.Y., Li, B., Quinlan, M.P., Takahashi, F., Maheswaran, S., McDermott, U., Azizian, N., Zou, L., Fischbach, M.A., et al. (2010). A chromatin-mediated reversible drug-tolerant state in cancer cell subpopulations. Cell *141*, 69–80.

Shechter, D., Dormann, H.L., Allis, C.D., and Hake, S.B. (2007). Extraction, purification and analysis of histones. Nat. Protoc. *2*, 1445–1457.

Stempor, P., and Ahringer, J. (2016). SeqPlots – interactive software for exploratory data analyses, pattern discovery and visualization in genomics. Wellcome Open Res. *1*, 14.

Stong, N., Deng, Z., Gupta, R., Hu, S., Paul, S., Weiner, A.K., Eichler, E.E., Graves, T., Fronick, C.C., Courtney, L., et al. (2014). Subtelomeric CTCF and cohesin binding site organization using improved subtelomere assemblies and a novel annotation pipeline. Genome Res. *24*, 1039–1050.

Teves, S.S., and Henikoff, S. (2012). Salt fractionation of nucleosomes for genome-wide profiling. Methods Mol. Biol. *833*, 421–432.

Vedadi, M., Barsyte-Lovejoy, D., Liu, F., Rival-Gervier, S., Allali-Hassani, A., Labrie, V., Wigle, T.J., Dimaggio, P.A., Wasney, G.A., Siarheyeva, A., et al. (2011). A chemical probe selectively inhibits G9a and GLP methyltransferase activity in cells. Nat. Chem. Biol. *7*, 566–574.

Vert, J.P., Foveau, N., Lajaunie, C., and Vandenbrouck, Y. (2006). An accurate and interpretable model for siRNA efficacy prediction. BMC Bioinformatics *7*, 520.

Vinogradova, M., Gehling, V.S., Gustafson, A., Arora, S., Tindell, C.A., Wilson, C., Williamson, K.E., Guler, G.D., Gangurde, P., Manieri, W., et al. (2016). An inhibitor of KDM5 demethylases reduces survival of drug-tolerant cancer cells. Nat. Chem. Biol. *12*, 531–538.

Wissing, S., Munoz-Lopez, M., Macia, A., Yang, Z., Montano, M., Collins, W., Garcia-Perez, J.L., Moran, J.V., and Greene, W.C. (2012). Reprogramming somatic cells into iPS cells activates LINE-1 retroelement mobility. Hum. Mol. Genet. *21*, 208–218.

Wu, T.D., and Nacu, S. (2010). Fast and SNP-tolerant detection of complex variants and splicing in short reads. Bioinformatics *26*, 873–881.

Zang, C., Schones, D.E., Zeng, C., Cui, K., Zhao, K., and Peng, W. (2009). A clustering approach for identification of enriched domains from histone modification ChIP-Seq data. Bioinformatics *25*, 1952–1958.

STAR★METHODS

KEY RESOURCES TABLE

REAGENT or RESOURCE	SOURCE	IDENTIFIER
Antibodies		
Rabbit monoclonal Histone 3 lysine 4 trimethyl	Cell Signaling	9751
Rabbit monoclonal Histone 3 lysine 9 dimethyl	Cell Signaling	4658
Rabbit polyclonal Histone 3 lysine 9 trimethyl	Abcam	ab8898
Rabbit monoclonal Histone 3 lysine 9 acetyl	Cell Signaling	9649
Rabbit polyclonal Histone 3 lysine 14 acetyl	EMD Millipore	07-353
Rabbit polyclonal Histone 3 lysine 18 acetyl	Cell Signaling	9675
Rabbit polyclonal Histone 3 lysine 23 acetyl	Cell Signaling	8848
Rabbit monoclonal Histone 3 lysine 27 trimethyl	Cell Signaling	9733
Rabbit monoclonal Histone 3 lysine 27 acetyl	Cell Signaling	8173
Rabbit monoclonal Histone 3	Cell Signaling	4499
Rabbit monoclonal anti-EMHT2/G9a	Cell Signaling	3306
Goat polyclonal anti-EMHT2/G9a	Santa Cruz Biotech	Sc-22879
Rabbit polyclonal anti-SETDB1	Bethyl Laboratories	A300-121A
Rabbit polyclonal anti-GAPDH	Thermo Fisher Scientific	PA1-987
Rabbit polyclonal anti-LINE1 ORF2	Santa Cruz Biotech	Sc-67197
Chicken polyclonal anti-LINE1 ORF2	LifeSpan Biosciences	LS-C130455
Mouse monoclonal anti-HDAC2	Cell Signaling	5113
Mouse monoclonal anti-HDAC3	Cell Signaling	3949
Mouse monoclonal anti-HDAC3	BD Transduction Labs	611124
Rabbit polyclonal anti-HP1-gamma	Cell Signaling	2619
Rabbit polyclonal anti-ATRX	Santa Cruz Biotech	15408
Rabbit polyclonal anti-H3.3	EMD Millipore	09-838
Mouse monoclonal anti-HA tag	Abcam	ab16918
Rabbit polyclonal Histone 3 lysine 27 acetyl	Abcam	ab4729
Rabbit polyclonal Histone 3 lysine 27 trimethyl	Active Motif	39155
Rabbit polyclonal anti-Jarid2	Abcam	Ab93288
Rabbit polyclonal anti-EHMT1/GLP	Bethyl Laboratories	A301-642A
Rabbit monoclonal anti-EZH2	Cell Signaling	5246
Rabbit monoclonal anti-SUZ12	Cell Signaling	3737
Rabbit polyclonal anti-EED	Millipore	09-774
Rabbit polyclonal anti-DNMT3L	Abcam	Ab3493
Rabbit polyclonal anti-Histone H1	Abcam	Ab61177
Rabbit polyclonal anti-H2Av	Active Motif	39715
Bacterial and Virus Strains		
IncuCyte® NucLight Red Lentivirus Reagent (EF-1 Alpha Promoter, Puromycin selection)	Essen Biosciences	4476
Biological Samples		
BRIM-2 trial patient samples for Nanostring	NCT00949702	McArthur et al., 2012
Chemicals, Peptides, and Recombinant Proteins		
Erlotinib	Synthesized at Genentech	N/A
GDC-0980 PI3 kinase inhibitor	Synthesized at Genentech	N/A
AZ628 (raf inhibitor)	Synthesized at Genentech	N/A
Lapatinib (HER2 inhibitor)	Synthesized at Genentech	N/A

(*Continued on next page*)

Continued

REAGENT or RESOURCE	SOURCE	IDENTIFIER
Crizotinib (ALK inhibitor)	Synthesized at Genentech	N/A
5-FU	Synthesized at Genentech	N/A
MS275 (HDAC inhibitor)	Synthesized at Genentech	From Syndax
UNC-0638 (G9a inhibitor)	Synthesized at Genentech	Vedadi et al., 2011
EPZ-6438 (EZH2 inhibitor)	Synthesized at Genentech	From Epizyme
GSK-126 (EZH2 inhibitor)	Synthesized at Genentech	From GSK
Trichostatin A	Sigma	T1952
Alpha-Amanitin	Sigma	A2263
SN-38	Sigma	H0165
Carboplatin	Sigma	C2538
5-Aza-2'-deoxycytidine	Sigma	189825
Zidovudine	Selleck Chemicals	S2579
Didanosine	Selleck Chemicals	S1702
HDAC1/2-selective G946	Synthesized at Genentech	Kattar et al., 2009
HDAC3-selective G877	Synthesized at Genentech	Rai et al., 2010
Puromycin	Calbiochem	540411
Doxycycline	Clontech	631311
Critical Commercial Assays		
Aldefluor Staining Kit	STEMCELL Technologies	01700
IncuCyte® Caspase-3/7 Apoptosis Assay Reagent	Essen Biosciences	0400
Taqman Fast Virus 1-Step Master Mix	Thermo Fisher	4444434
iScript cDNA synthesis kit	Bio-Rad	1708890
Taqman PreAmp Master Mix	Thermo Fisher	4391128
RNeasy mini kit	Qiagen	74104
SuperScript III Platinum SYBR Green One-Step qRT-PCR Kit with ROX	Thermo Fisher	11746100
Histone Purification Mini Kit	Active Motif	40026
Vybrant DyeCycle Green Nuclear Stain	Thermo Fisher	V35004
Nuclear-ID Red DNA stain	Enzo Biosciences	ENZ-52406
DNeasy Blood and Tissue Kit	Qiagen	69504
Cyquant Reagent	Thermo Fisher	C7026
Deposited Data		
ATACseq	Geo	GSE74180
RNAseq	Geo	GSE74180
ChIPSeq	Geo	GSE74180
Proteomics data	Peptide atlas	PASS01054
Experimental Models: Cell Lines		
PC9 (NSCLC)	Genentech Cell Bank	N/A
SW480 (Colorectal)	Genentech Cell Bank	N/A
SKBR3 (Breast)	Genentech Cell Bank	N/A
M14 (Melanoma)	Genentech Cell Bank	N/A
Hs888 (Melanoma)	Genentech Cell Bank	N/A
C32 (Melanoma)	Genentech Cell Bank	N/A
Colo205 (Colon)	Genentech Cell Bank	N/A
EVSAT (Breast)	Genentech Cell Bank	N/A
GTL-16 (Gastrointestinal)	Genentech Cell Bank	N/A
Experimental Models: Organisms/Strains		
NOD/SCID mice	Charles River Labs	394

(*Continued on next page*)

Continued

REAGENT or RESOURCE	SOURCE	IDENTIFIER
Oligonucleotides		
L1-ORF1-1 (SYBR Green) Forward: 5'- TCAAAGGAAAGCCCATCAGACTA -3' Reverse: 5'- TGGCCCCCACTCTCTTCT -3'	Synthesized at Genentech	(Guo et al., 2014)
L1-ORF1-2 (SYBR Green) Forward: 5'- GGTTACCCTCAAAGGAAAGCC -3' Reverse: 5'- GCCTGGTGGTGACAAAATCTC -3'	Synthesized at Genentech	(Chen et al., 2012)
L1-5'UTR (SYBR Green) Forward: 5'- ACGGAATCTCGCTGATTGCTA -3' Reverse: 5'- AAGCAAGCCTGGGCAATG -3'	Synthesized at Genentech	(Guo et al., 2014)
L1-ORF2 (SYBR Green) Forward: 5'- AAATGGTGCTGGGAAAACTG -3' Reverse: 5'- GCCATTGCTTTTGGTGTTTT -3'	Synthesized at Genentech	(Chen et al., 2012)
Beta-actin (SYBR Green) Forward: 5'- GGCATGGGTCAGAAGGATT -3' Reverse: 5'- GGGGTGTTGAAGGTCTCAAA -3'	Synthesized at Genentech	(Guo et al., 2014)
L1-5'UTR-1 Forward: 5'-GAATGATTTTGACGAGCTGAGAGAA-3' Reverse: 5'-GTCCTCCCGTAGCTCAGAGTAATT-3' Probe: 5'-AAGGCTTCAGACGATC-3'	Synthesized at Genentech	(Coufal et al., 2009)
L1-5'UTR-2 Forward: 5'-ACAGCTTTGAAGAGAGCAGTGGTT-3' Reverse: 5'-AGTCTGCCCGTTCTCAGATCT-3' Probe: 5'- FAM-TCCCAGCACGCAGC-BHQ-3'	Synthesized at Genentech	(Wissing et al., 2012)
L1-ORF1 Forward5'-TCAAAGGAAAGCCCATCAGACTA-3' Reverse 5'-TTGGCCCCCACTCTCTTCT-3' Probe: 5'- FAM-CAGCGGATCTCTCGG-BHQ-3'	Synthesized at Genentech	(Wissing et al., 2012)
L1-ORF2 Forward: 5'-GGATGGCTGGGTCAAATGGT-3' Reverse: 5'-GAGAGGATGCGGAGAAATAGGA-3' Probe:5'-FAM CAACCATTGTGGAAGTCAGTGTGGCG-BHQ-3'	Synthesized at Genentech	(Wissing et al., 2012)
ERCC RNA spike-in mix 1 Taqman probe	Life Technologies	(Ac03459872_a1)
β-actin Taqman Assay	Life Technologies	(Hs01060665_g1)
G9a/EHMT2 Taqman Assay	Life Technologies	(Hs00198710_m1)
GAPDH Taqman Assay	Life Technologies	(Hs02758991_g1)
SUV39H1 Taqman Assay	Life Technologies	(Hs00957892_m1)
SUV39H2 Taqman Assay	Life Technologies	(Hs00226596_m1)
GLP/EHMT1 Taqman Assay	Life Technologies	(Hs00964325_m1)
SETDB1 Taqman Assay	Life Technologies	(Hs01048361_m1)
EZH1 Taqman Assay	Life Technologies	(Hs00940463_m1)
EZH2 Taqman Assay	Life Technologies	(Hs00544830_m1)
EED Taqman Assay	Life Technologies	(Hs00537777_m1)
SUZ12 Taqman Assay	Life Technologies	(Hs00248742_m1)
Jarid2 Taqman Assay	Life Technologies	(Hs01004467_m1)
Rig-1/DDX58 Taqman Assay	Life Technologies	(Hs01061436_m1)
IFIH1 Taqman Assay	Life Technologies	(Hs00223420_m1)
IRF7 Taqman Assay	Life Technologies	(Hs01014809_g1)
OASL Taqman Assay	Life Technologies	(Hs00984387_m1)
LINE siRNA1 5'-TCAGCAATGGAAGATGAAATGAATG-3'	Synthesized at Genentech	(Aschacher et al., 2016)
LINE siRNA2 5'-AAGAAATGAGCAAAGCCTCCAAGAA-3'	Synthesized at Genentech	(Aschacher et al., 2016)

(*Continued on next page*)

Continued

REAGENT or RESOURCE	SOURCE	IDENTIFIER
LINE siRNA3 5'-GAAATGAAGCGAGAAGGGAAGTTTA-3'	Synthesized at Genentech	(Aschacher et al., 2016)
Scrambled siRNA 5'-GAAGAAGGAGCGGAAGAAGTTATTA-3'	Synthesized at Genentech	(Aschacher et al., 2016)
Rig-1/DDX58-1 siRNA sense strand	Sigma	SASI_HS01_00047983
Rig-1/DDX58-2 siRNA sense strand	Sigma	SASI_HS01_00047980
Rig-1/DDX58-3 siRNA sense strand	Sigma	SASI_HS02_00345407
G9a/EHMT2 CRSPR guide RNAs CCCTCAGTGTGCTCCCTCT; CTGGAGAAACTGCAAGAAC	Synthesized at Genentech	(Cong et al., 2013
H3F3B CRSPR guide RNAs GATTCAGAGGTCCCGACGC; TGTAGGCGGCTTCCTGTAT	Synthesized at Genentech	(Jinek et al., 2013)
EZH2 CRSPR guide RNAs GGTTTGTTCACTTCAGAACTTGG; AAGACCCCACCAAAACGTCCAGG	Synthesized at Genentech	(Mali et al., 2013)
Primers used to determine WT G9a/EHMT2 allele: WT G9a-Fwd (TCCTCTTCTTCTTCCTCTTCC) WT G9a-Rev (CCAGTAAAAAGAACAATCACTATTC)	Synthesized at Genentech	N/A
Primers used to determine deletion events in the G9a/EHMT2 gene: KO G9a-Fwd (AAGACAAGCTCTGTGGTCTGG) KO G9a-Rev (AAAATGTGGCATTTATAC)	Synthesized at Genentech	N/A
Primers used to determine WT EZH2 allele: WT EZH2-Fwd (GACTGAAGAAAGAACTTATCATCT) WT EZH2-Rev (CATAATTTTCTCTGGGTAATGC)	Synthesized at Genentech	N/A
Primers used to determine deletion events in EZH2 gene: KO EZH2-Fwd (AAGATAGTGGGTGCATTAAAA) KO EZH2-Rev (TAGAACTTTGCCCTGATGTT)	Synthesized at Genentech	N/A
SETDB1 sh3 forward: TCGAGAAGGTATATTGCTGTTGACAGTGAGCGATAGCTGAGACACCA AACGTCATAGTGAAGCCACAGATGTATGACGTTTGGTGTCTCAGCTAG TGCCTACTGCCTCGGACTTCAAGGGGCTAG SETDB1 sh3 reverse: AATTCTAGCCCCTTGAAGTCCGAGGCAGTAGGCACTAGCTGAGACACCA AACGTCATACATCTGTGGCTTCACTATGACGTTTGGTGTCTCAGCTATCG CTCACTGTCAACAGCAATATACCTTC	Synthesized at Genentech	N/A
SETDB1 sh4 forward: TCGAGAAGGTATATTGCTGTTGACAGTGAGCGAACCTGATAGTCAGCATG CGAATAGTGAAGCCACAGATGTATTCGCATGCTGACTATCAGGTGTGCCT ACTGCCTCGGACTTCAAGGGGCTAG SETDB1 sh4 reverse: AATTCTAGCCCCTTGAAGTCCGAGGCAGTAGGCACACCTGATAGTCAGCA TGCGAATACATCTGTGGCTTCACTATTCGCATGCTGACTATCAGGTTCGCT CACTGTCAACAGCAATATACCTTC	Synthesized at Genentech	N/A
Ren. 713 forward: TCGAGAAGGTATATTGCTGTTGACAGTGAGCGAAGGAATTATAATGCTTAT CTATAGTGAAGCCACAGATGTATAGATAAGCATTATAATTCCTGTGCCTAC TGCCTCGGACTTCAAGGGGCTAG Ren. 713 reverse: AATTCTAGCCCCTTGAAGTCCGAGGCAGTAGGCACAGGAATTATAATGCTT ATCTATACATCTGTGGCTTCACTATAGATAAGCATTATAATTCCTTCGCTCA CTGTCAACAGCAATATACCTTC	Synthesized at Genentech	N/A
Recombinant DNA		
pMinDUCER-tRFP-miRE-EIP	Genentech	N/A
pLKO-SHC201-gRNA-GNE	Genentech	N/A
pRK-TK-Neo-Cas9-HA	Genentech	N/A

(*Continued on next page*)

Continued

REAGENT or RESOURCE	SOURCE	IDENTIFIER
Software and Algorithms		
Bowtie		Langmead et al., 2009
BWA version 0.7.12		
MACS 1.4.2		Gal-Yam et al., 2008)
SICER		Zang et al., 2009
RepeatMasker	UCSC	
GSNAP		Wu and Nacu, 2010
Salmon		Patro et al., 2017
Bioconductor package edgeR		Robinson et al., 2010
Vomm-Limma		Law et al., 2014
Skyline		https://skyline.ms

CONTACT FOR REAGENT AND RESOURCE SHARING

Requests for further information and resources may be directed to lead contact Marie Classon (classon.marie@gmail.com) or Catherine Wilson (Wilson.catherine@gene.com).

EXPERIMENTAL MODEL AND SUBJECT DETAILS

Cell Lines and Genomic Annotations

All cell lines including PC9, EVSAT, Colo205, C32, M14, Hs888 and SW480 and their derivatives are routinely genotyped by the Genentech cell culture banking facility to ensure their identity.

Cell Culture Conditions

PC9, EVSAT, Colo205, C32, M14, Hs888 and SW480 cells were maintained at 37°C with 5% CO_2 in high glucose RPMI1640 containing 10% heat inactivated Fetal Bovine Serum (FBS). GTL-16 cells were cultured in RPMI 1640 supplemented with 5% FBS and SKBR3 cells were cultured in F12:DMEM (50:50) media with 10% FBS.

Mouse Xenograft Experiments

All experiments were conducted using *NOD/SCID* mice and were approved and monitored by the Institutional Animal Care and Use Committee at Genentech Inc.

Patient Samples

BRIM2 (NCT00949702) (McArthur et al., 2012) was a single-arm phase 2 clinical study in which patients with metastatic melanoma carrying a BRAFV600E mutation received vemurafenib. Patient consent was obtained for exploratory research conducted on all tissues. The protocol was approved by the institutional review board at each participating institution, and the study was conducted in accordance with the protocol and the ethical principles of the Declaration of Helsinki. All study participants provided written informed consent.

METHOD DETAILS

Inhibitors Used

EGFR inhibitor erlotinib, dual PI3K/mTOR inhibitor GDC-0980, pan-Raf inhibitor AZ628, B-Raf inhibitor PLX-4032, dual HER2/EGFR inhibitor lapatinib, ALK inhibitor crizotinib, 5-FU, MS275 (HDAC inhibitor, Syndax), G946 (Kattar et al., 2009), G877 (Rai et al., 2010), UNC-0638 (G9a inhibitor, Vedadi et al., 2011), GSK-126 (EZH2 inhibitor, GlaxoSmithKline) and EPZ-6438 (EZH2 inhibitor, Epizyme) were synthesized at Genentech. The RT-i: Zidovudine and Didanosine were purchased from Selleck Chemicals. TSA, α-amanitin, SN-38, 5-Aza-2'-deoxycytidine and carboplatin were purchased from Sigma.

DTP Generation

Cancer cell lines were treated with 1 μM erlotinib (erl) for 7-9 days (PC9); 2 μM GDC-0980 for 9 days (EVSAT); 2 μM AZ628 for 9 days (Colo205); 1 μM lapatinib for 12-15 days (SKBR3), 2 μM PLX-4032 for 15 days (C32), 33 μM 5-FU and 6nM SN-38 for 14 days (SW480), 1 μM crizotinib for 4 weeks (GTL-16) or 2 μM AZ628 for 14 days (Hs888 and M14). Media supplemented with the relevant drug was replaced every 3-4 days. Cells that survived treatment for the number of days specified above for each cell line model were considered DTPs.

Immunoblotting

All immunoblotting was performed following SDS-PAGE using standard methods. Antibodies used were: H3K4me3 (Cell Signaling 9751), H3K9me2 (Cell Signaling 4658), H3K9me3 (Abcam ab8898), H3K9Ac (Cell Signaling 9649), H3K14Ac (Millipore 07-353), H3K18Ac (Cell Signaling 9675), H3K23Ac (Cell Signaling 8848), H3K27me3 (Cell Signaling 9733), H3K27Ac (Cell Signaling 8173), Histone H3 (Cell Signaling 4499), G9a (Cell Signaling 3306), G9a (Santa Cruz sc-22879), SETDB1 (Bethyl A300-121A), GLP (Bethyl A301-642A), Jarid2 (Abcam ab93288), EZH2 (Cell Signaling 5246), SUZ12 (Cell Signaling 3737), EED (Millipore 09-774), DNMT3L (Abcam ab3493), Histone H1 (Abcam ab61177), GAPDH (Pierce PA1-987), LINE-1ORF2 (H-110 Santa Cruz sc-67197), LINE-1ORF2 (LSBio LS-C130455), HDAC2 (Cell Signaling 5113), HDAC3 (Cell Signaling 3949), HDAC3 (BD Transduction Labs 611124), HP1-γ (Cell Signaling 2619), ATRX (Santa Cruz sc-15408), H3.3 (Millipore 09-838) and anti-HA tag (Abcam ab16918).

Immunofluorescence and Immunohistochemistry Using Xenograft Tumor Material

PC9 vehicle or erl-treated PC9 xenograft tumors formed in *NOD/SCID* mice were cut into 10 μm frozen sections. Sections were dried on slides. Prior to fixation, sections were re-hydrated with PBS for 5 minutes. Samples were fixed with 4 % formaldehyde at 25^0 C for 10 min. Cells were washed with PBS, permeabilized, incubated in blocking buffer (2% BSA, 0.3% Triton-X and 3% goat serum in PBS) at room temperature for one hour, followed by an incubation with primary antibody (α-H3K27ac Abcam ab4729, α-H3K27me3 Active Motif 39155) at 4°C overnight. Following 3 washes in blocking buffer, cells were incubated with secondary antibodies (Alexafluor 594 conjugated anti-mouse or anti-rabbit at 0.5 μg/ml) at room temperature for 45 minutes, washed once with blocking buffer and stained with Hoechst (1:5000) for 10 minutes prior to mounting using Vectashield (Vector Labs) and imaged with INCell6000 (GE Healthcare). In this experiment PC9 cells expression nuclear RFP was used (Essen Biosciences). H3K27me3, H3K27ac signals were quantified using INCell Developer Toolbox analysis software (GE Healthcare). H3K27me3 and H3.3 immunohistochemistry (IHC) was performed by incubating the tissue section slides at room temperature for 60 minutes using the rabbit monoclonal anti-H3K27me3 antibody (Cell Signaling 9733), and the rabbit polyclonal anti-H3.3 antibody (Millipore 09-838), respectively (both tested for IHC specificity). Heat-induced epitope retrieval was performed with target antigen retrieval buffer (Dako). The immunoreaction was detected with 5 μg/ml biotinylated donkey anti-rabbit IgG in concert with the Vectastain Elite ABC-Peroxidase system (Vector Labs) and DAB chromogen. Tissues sections were counterstained with hematoxylin. Whole slide digital images of each immune-labeled tissue section were obtained using a Nanozoomer digital slide scanner (Hamamatsu). Tumor areas were either manually annotated or automatically segmented using the MatLab (MathWorks) software package. MatLab was subsequently used to identify tumor cell nuclei based on size, shape and labeling characteristics and calculate the average intensity of DAB labeling of each nuclei. Nuclei were subsequently binned as weak positive, moderate positive, and strong positive according to DAB intensity thresholds. Final immunolabeling quantification results were reported as percent strong positive cells/ total cells or as H-score, calculated as the sum of percentage of cells that have strong staining multiplied by 300, percentage of cells that have medium labeling multiplied by 200 and percentage of cells that have weak staining multiplied by 100.

Aldefluor Staining

For FACS studies of ALDH positive cells, PC9 cells were stained using an Aldefluor kit (STEMCELL Technologies) according to the manufacturer's recommendations. Following staining (0.5 millions cells/mL with 5 μL reagent), cells were sorted using a FACS Aria cell sorter. The brightest (5%) cells were designated as the Aldefluor $(ALDH)^{High}$ population, whereas cells with the dimmest (5%) Aldefluor staining were collected as Aldefluor $(ALDH)^{Low}$ population.

Epigenetic Inhibitor Cell Assays

For G9a and EZH2 inhibitor experiments, cells were treated with a G9a inhibitor (UNC-0638) or the EZH2 inhibitors (EPZ-6438 and GSK126) at indicated concentrations for 5 days, and then plated in 6-well dishes in media supplemented with or without the targeted drugs (in 5% FBS) in combination with the G9a or EZH2 inhibitor. Media and drugs were changed every 2-3 days for the indicated number of days. At the end of the experiment the number of remaining cells was counted for each parental and DTP model. Each 6-well was analyzed using imaging and analysis software from Essen Bioscences (IncuCyteZoom) to count remaining live cells (DTPs) after staining with Nuclear-ID Red DNA stain dye (Enzo Life Sciences) or by the use of PC9-RFP transduced cells when indicated. For each well of 6-well plates, 36 images were acquired and the average number of nuclei in each image was calculated. Each experiment was run in triplicate. For experiments with MS275 (entinostat, HDAC inhibitor), PC9DTPs were treated with indicated concentrations of MS275 and cells were analyzed by imaging by IncuCyteZoom in triplicate on day 3,7 and 9 following addition of MS275. Media and drugs were changed every 2-3 days. For HDAC inhibitor assays using HDAC1/2-selective G946 (Terephthalamide SAR) (Kattar et al., 2009) or HDAC3-selective G877 (Compound 136) (Rai et al., 2010), PC9 cells were seeded in 6-well plates and treated with 1 μM erl and the HDAC inhibitors for 30 days, after which the plates were stained with Giemsa. For experiments with TSA, cells were treated as indicated with 25 or 50 nM TSA. The experiments with 5-Aza-2'-deoxycytidine (Aza) were performed as indicated in the figure legend (Figures S2P and S2Q) with combined treatment with 1 μM erl -/+low doses of 5-Aza as indicated in the figure. Media and drugs were changed every 2-3 days. In all cases the amount/mL media of DMSO was the same.

Xenograft Studies

For the TSA experiment: *NOD/SCID* mice were inoculated subcutaneously in the right flank with 5 million PC9 cells in HBSS:Matrigel, in a volume of 100 μl. When mean tumor volume reached 100-200 mm^3, 72 mice were placed into groups with equivalent mean tumor

volumes (n=12 per group). Groups were treated as follows: Group 1: Captisol Vehicle orally (PO) daily; 5 days/week for 3 weeks. Group 2: erl 30 mg/kg PO daily; 5 days/week for 7 weeks. Group 3: TSA 0.5 mg/kg subcutaneously (SQ) daily; 5 days/week for 3 weeks. Group 4: erl 30 mg/kg PO for 10 days and TSA 0.5 mg/kg SQ daily; 5 days/week for 6 weeks. For the MS275 experiment: *NOD/SCID* mice were inoculated subcutaneously in the right flank with 5 million PC9 cells in HBSS:Matrigel, in a volume of 100μl. When mean tumor volume reached 100-200 mm^3, 72 mice were placed into groups with equivalent mean tumor volumes (n=12 per group). Groups were treated as follows: Group 1: Captisol vehicle orally in Medidrop, daily to end of study. Group 2: erl (30 mg/kg) orally in Medidrop daily for 10 days. Group 3: MS-275 40 mg/kg intraperitoneally (IP) daily from day 10 to end of study. Group 4: erl (30 mg/kg) orally in Medidrop daily for ten days + MS-275 (40 mg/kg) IP daily from day 10 to end of study. For the IHC and IF experiments: *NOD/SCID* mice were inoculated subcutaneously in the right flank with 5 million PC9 cells in HBSS:Matrigel, in a volume of 100 μl. When mean tumor volume reached 100-200 mm^3, groups were treated as follows: Group 1: Captisol Vehicle orally (PO) daily; 5 days/week for 9 days. Group 2: erl 30 mg/kg PO daily; 5 days/week for 9 days after which the tumors were fixed and processed for IHC. For the experiment with wild-type and *EHMT2/G9a* knock-out cells: *NOD/SCID* mice were inoculated subcutaneously in the right flank with 5 million cells in HBSS:Matrigel, in a volume of 100 μl. Electronic caliper assessment of tumor size as well as mouse weights were measured every 3-4 days (n=10 animals/group). Animal experiments were approved by the Institutional Animal Care and Use Committee at Genentech Inc.

Reverse Transcriptase Inhibitor Studies

PC9-RFP (PC9 cells stably transduced with a RFP expressing vector according to the manufacturers recommendations (NucLight Red Essen Biosciences, 4478) cells were seeded at equal densities in 6-well plates in triplicate in 1 μM erl for 4 days with a media change on day 3. Thereafter, the remaining PC9DTPs were separated into 4 subgroups: (1) 1 μM erl +DMSO, (2) 1 μM erl plus 50 μM Zidovudine and 50 μM Didanosine, (3) 1 μM erl and 50 nM TSA and (4) 1 μM erl, 50 μM Zidovudine, 50 μM Didanosine and 50 nM TSA. Treatments continued for 4 days before all drugs except 1 μM erl were removed. Cells were maintained in the presence of 1 μM erl for 10 days to more accurately capture the number of cells that remain after TSA-induced ablation of DTPs. For the experiment in Figure 7D the cells were plated in the indicated drugs for 3 days after which the remaining cells were analyzed. All cell analysis was performed in triplicate using IncuCyteZoom. For each well of 6-well plates, 36 images were acquired and the average number of nuclei in each image was calculated. For regrowth assays the cells were maintained in 1 μM erl for an additional 15-40 days (as indicated) after which the cells were fixed in paraformaldehyde and stained with Giemsa stain.

Caspase-3/7 Cleavage Assay

PC9-RFP cells were plated at equal densities in 6-well plates in triplicate with and without 1 μM erl for four days. On day three of this experiment parental PC9-RFP cells were plated at $1x10^5$ cells per well in 6-well plates in triplicate. On day four for erl-treated cells and day two for parental cells, 50 nM TSA plus 5 μL of IncuCyte Caspase-3/7 reagent (Essen Biosciences 4440) were added to PC9 parental cells and PC9DTPs. Plates were imaged by IncuCyteZoom every three hours for 72 hours in phase contrast, red and green channels according to the manufacturer's recommendations. Erl-induced death continues throughout the assay (i.e., the DTP population is not uniform and contains a population that is responding to erl even after several rounds of treatment). In order to separate the erl-induced death from the TSA-induced death, the erl-induced caspase activation signal was subtracted from the TSA-induced caspase activation signal at each time point to generate graphs representing TSA-induced caspase activation. The caspase activation signal is represented as the number of green cells divided by the number of green cells plus the number of red cells to incorporate all cells in the analysis.

siRNA Screen

Dharmacon siGenome siRNAs were used at a final concentration of 12.5 nM for single siRNAs to target each of 298 genes involved in epigenetic regulation (Tables S3). The screen was run twice in duplicate. PC9 cells were reverse-transfected with the arrayed siRNAs using Dharmafect 1 reagent (Dharmacon). Dharmafect 1 was chosen for this cell line due to high transfection efficiency and low toxicity. Briefly, individual arrayed siRNAs were mixed with a master mix of OPTI-MEM (Invitrogen) and Dharmafect 1 (Dharmacon) and subsequently incubated at room temperature for 45 minutes. siRNA:lipid mixtures were added to each well prior to addition of a PC9 cell suspension at a final cell density of 1000 cells/well. After 48 hours, the transfection medium was removed and replaced with medium containing DMSO or 1 μM erl. Following 72 hour erl treatment, cells were allowed to recover for 72 hour, after which 100 μl of Cyquant reagent was added to each well and incubated for 1 hour prior to capturing fluorescence images on the InCell 2000 (GE Healthcare) at 4x magnification. The number of nuclei per well was determined using GE Developer software. Performance of the assays was evaluated calculating the z factor comparing the DMSO and the erl treated cells (z factor > 0.75) and the erl/non-targeting control (NTC) versus the erl/positive control (HDAC3 siRNA, z factor > 0.6). Assay results were analyzed using ScreenSifter and z scores calculated for each record as described (Kumar et al., 2013). Hits were selected based on the effect of each individual siRNA, with at least 2-3 siRNAs significantly reducing the number of cells in the presence of erl and having no effect on cells in media alone compared to the non-targeting control (NTC). For the data presented in Figures 2B–2D and S2A error bars represent +/-SD of the fold changes of each siRNA (n=4, 2 per screen) as compared to the NTC control (n=16, 8/screen) for each experiment, and p values were generated based on fold changes comparing each siRNA to NTC using paired t-test.

siRNA Knock-Down of LINE-1 elements and Rig-1/DDX58

For individual knock down, PC9 cells were transfected at 12.5 nM final concentration with Dharmafect 1 (Dharmacon) reagent in optiMEM. siRNAs used to target young LINE elements (Aschacher et al., 2016) were:

LINE siRNA1: (5'-TCAGCAATGGAAGATGAAATGAATG-3'),
LINE siRNA2: (5'-AAGAAATGAGCAAAGCCTCCAAGAA-3'),
LINE siRNA3: (5'-GAAATGAAGCGAGAAGGGAAGTTTA-3')
Scrambled siRNA: (5'-GAAGAAGGAGCGGAAGAAGTTATTA-3')
siRNAs used to target Rig-1/DDX58 were purchased from Sigma:
Rig-1/DDX58-1 (SASI_HS01_00047983, sense strand)
Rig-1/DDX58-2 (SASI_HS01_00047980, sense strand)
Rig-1/DDX58-3 (SASI_HS02_00345407, sense strand)

For DTP experiments, PC9 cells transfected with siRNAs, as described above, were treated with 1 μM erl in the presence of 25 nM TSA for 7 days, starting at 48 hours post-siRNA transfection. Media was replaced with fresh media supplemented with 1 μM erl and 25 nM TSA every 3 days. Live cells were counted on day 7 by imaging on IncuCyteZoom (36 images per well in 6-well dish). Average number of cells per image for each was calculated from two biological replicates that were run in technical triplicates.

CRISPR-mediated Gene Targeting of *G9a/EHMT2/KMT1C*, *EZH2* and *H3F3B*

PC9 cells were transiently transfected with plasmids expressing Cas9 and guide RNAs targeting the indicated genes (Cong et al., 2013; Jinek et al., 2013; Mali et al., 2013). Guide RNAs used for G9a/EHMT2/KMT1C, EZH2 and H3F3B (H3F3B is more highly expressed than H3F3A in PC9 cells, data not shown):

G9a: CCCTCAGTGTGCTCCCTCT; CTGGAGAAACTGCAAGAAC
H3F3B: GATTCAGAGGTCCCGACGC; TGTAGGCGGCTTCCTGTAT.
EZH2: GGTTTGTTCACTTCAGAACTTGG; AAGACCCCACCAAAACGTCCAGG

Six days following transfection, cells were seeded in 96-well plates for single cell cloning. G9a clones were analyzed for *G9a/EHMT2/KMT1C* gene content by PCR after DNA isolation using DNeasy Blood and Tissue kit (Qiagen).

PCR primers pairs used to determine the presence of WT *G9a* allele were:
WT G9a-Fwd (TCCTCTTCTTCTTCCTCTTCC)
WT G9a-Rev (CCAGTAAAAAGAACAATCACTATTC).
PCR primers used to confirm deletion events in the *G9a/EHMT2/KMT1C* gene were:
KO G9a-Fwd (AAGACAAGCTCTGTGGTCTGG)
KO G9a-Rev (AAAATGTGGCATTTATAC).
Loss of G9a protein expression was also confirmed by immunoblotting and histone MS alterations in H3K9 methylation.
PCR primer pairs used to determine the presence of the WT *EZH2* allele were:
WT EZH2-Fwd (GACTGAAGAAAGAACTTATCATCT)
WT EZH2-Rev (CATAATTTTCTCTGGGTAATGC)
PCR primers used to confirm deletion events in the *EZH2* gene were:
KO EZH2-Fwd (AAGATAGTGGGTGCATTAAAA)
KO EZH2-Rev (TAGAACTTTGCCCTGATGTT).
Loss of EZH2 protein was also confirmed by immunoblotting and histone MS of lost H3K27 methylation.

Reduced expression of H3.3 was measured using an H3.3 specific antibody. For H3.3 rescue experiments, a *H3F3B* CRISPR clone was complemented with H3.1 or H3.3 expression by stable lentiviral transduction using pReceiver-Lv120 constructs, expressing H3.1 or H3.3 under CMV promoter with a C-terminal 3xHA-tag. Expression was confirmed using anti-Histone H3.3 (Millipore 09-838) and anti-HA tag (Abcam ab16918) antibodies.

Inducible shRNA Knock-down of SETDB1

A lentiviral, doxycycline (DOX)-inducible shRNA expression vector, pMinDUCER-tRFP-miRE-EIP, was constructed through conversion of the pLKO.5 backbone (Sigma-Aldrich) using synthetic gene fragments (GenEscript). The full pMinDUCER_tRFP-miRE-EIP vector sequence is available upon request. Individual shRNAs targeting human SETDB1 were designed using the DSIR algorithm (Vert et al., 2006). All targeting sequences were converted into 125 nt DNA oligonucleotides, annealed, and cloned into the XhoI-EcoRI restriction sites, enabling expression of optimized miR-30-based shRNAs along with the turboRFP marker. Below are the oligo sequences used:

SETDB1-sh3_(forward): TCGAGAAGGTATATTGCTGTTGACAGTGAGCGATAGCTGAGACACCAAACGTCATAGTGAAGCCACAGATGTATGACGTTTGGTGTCTCAGCTAGTGCCTACTGCCTCGGACTTCAAGGGGCTAG
SETDB1-sh3_(reverse): AATTCTAGCCCCTTGAAGTCCGAGGCAGTAGGCACTAGCTGAGACACCAAACGTCATACATCTGTGGCTTCACTATGACGTTTGGTGTCTCAGCTATCGCTCACTGTCAACAGCAATATACCTTC
SETDB1-sh4_(forward): TCGAGAAGGTATATTGCTGTTGACAGTGAGCGAACCTGATAGTCAGCATGCGAATAGTGAAGCCACAGATGTATTCGCATGCTGACTATCAGGTGTGCCTACTGCCTCGGACTTCAAGGGGCTAG
SETDB1-sh4_(reverse): AATTCTAGCCCCTTGAAGTCCGAGGCAGTAGGCACACCTGATAGTCAGCATGCGAATACATCTGTGGCTTCACTATTCGCATGCTGACTATCAGGTTCGCTCACTGTCAACAGCAATATACCTTC

Ren.713_(forward): TCGAGAAGGTATATTGCTGTTGACAGTGAGCGAAGGAATTATAATGCTTATCTATAGTGAAGCCACAGATGT ATAGATAAGCATTATAATTCCTGTGCCTACTGCCTCGGACTTCAAGGGGCTAG

Ren.713_(reverse): AATTCTAGCCCCTTGAAGTCCGAGGCAGTAGGCACAGGAATTATAATGCTTATCTATACATCTGTGGCTTCA CTATAGATAAGCATTATAATTCCTTCGCTCACTGTCAACAGCAATATACCTTC

Production of control and SETDB1-sh virus: 293T cells were plated one day prior to Lipofectamine 2000 transfection with 5 μg of expression plasmid, 10 μg delta8.9 and 0.5 μg VSVG. After 6 hours at 37°C the media was removed and replenished with fresh growth media. Media was harvested at 24 and 48 hours after transfection and cleared by centrifugation. These viral supernatants were then used to infect target cells. SW480 cells were plated in 96-well plates one day prior to infection using 40 μL of viral supernatant with 8 μg/mL Polybrene (Millipore TR-1003-G) and incubated overnight before media was changed and replaced with fresh growth media. 48 hours after infection the cells were placed in selection media containing 1μg/mL puromycin (Calbiochem 540411) for 2 weeks. The stable pool of infected SW480 cells was then treated with 250 ng/mL doxycycline (DOX, Clontech 631311) to confirm RFP expression. Knock-down of SETDB1 was confirmed by qRT-PCR as well as western blot using conditions described. SW480 virally transduced with NTC, SETDB1-sh3 or SETDB1-sh4 were pretreated for 5 days with 250 ng/mL doxycycline (DOX) prior to being plated $1x10^5$ cells per well of a six-well plate in triplicate. The next day fresh media was added with 33 μM 5-FU and 6 nM SN-38. Cells were treated with either one or three changes of media containing drug before surviving cells were stained with Vybrant DyeCycle green nuclear stain (Life Technologies V35004) and quantitated using IncuCyteZoom. For each well of 6-well plates, 36 images were acquired and the average number of nuclei in each image was calculated. For cell regrowth experiments, drug was removed after one or three media changes and then left to regrow for 40 days after which the remaining cells were stained with Giemsa stain.

Subcellular Fractionation

Fractionation was performed as described (Mendez and Stillman, 2000). Briefly, 3 x 10^6 cells were re-suspended in 200 μl of Buffer A (10 mM HEPES pH7.9, 10 mM KCl, 1.5 mM $MgCl_2$, 0.34 M sucrose, 10% glycerol, 1 mM DTT, 1x HALT protease and phosphatase inhibitor) prior to adding Triton-X-100 at a final concentration of 0.1%. Nuclei were pelleted at 1300 x g at 4°C for 4 minutes, and the supernatant was saved as the cytoplasmic fraction. The nuclear pellet was washed once by re-suspending in 200 μl Buffer A without Triton-X-100, followed by centrifugation at 1300 x g at 4°C for 4 minutes. The nuclear pellet was re-suspended in Buffer B (3 mM EDTA, 0.2 mM EGTA, 1 mM DTT, 1x HALT protease and phosphatase inhibitors), incubated on ice for 30 minutes, after which the chromatin fraction was pelleted by centrifugation at 1700 x g at 4°C for 4 minutes. Supernatant was saved as the nuclear-soluble fraction. The chromatin pellet was washed once by re-suspension in 200 μl Buffer B followed by centrifugation at 1700 x g at 4°C for 4 minutes and sonicated in 1x SDS-PAGE loading buffer 35 cycles of 20 sec ON and 30 sec OFF using a Diagenode Bioruptor.

Salt Fractionation

Salt fractionations were performed as described (Teves and Henikoff, 2012) with minor modifications. Briefly, cells were resuspended in TM2 buffer (10 mM Tris–HCl, pH 7.4, 2 mM $MgCl_2$ 2, 0.5 mM phenylmethylsufonyl fluoride (PMSF), then lysed by adding Nonidet P-40 (NP-40) to a final concentration of 0.1%, then kept on ice for 3 minutes while vortexing for 5 seconds every minute. Thereafter, the suspension was spun at 100xg for 10 minutes to pellet the nuclei, and subsequently washed with TM2 buffer. The nuclei were resuspended in TM2 buffer and $CaCl_2$ and MNase were added to a final concentration of 1 mM and 1.25 U/mL, respectively. Following incubation at 37°C for 10 minutes, MNase digestion was stopped by addition of EGTA to a final concentration of 2 mM. An aliquot was removed and designated as nuclei. The remained of the digested nuclei was resuspended in Triton buffer (10 mM Tris–HCl, pH7.4, 2 mM $MgCl_2$, 2 mM EGTA, 0.1% Triton X-100, 0.5 mM PMSF) with increasing salt concentrations as indicated in the figure (80 mM, 150 mM, or 600 mM NaCl). After 2 hours at 4°C, suspensions were spun at 100xg for 10 minutes and the resulting supernatant was saved in a fresh tube while the pellet was resuspended in TNE buffer (10 mM Tris–HCl, pH 7.4, 200 mM NaCl, 1 mM EDTA). The pellet and the soluble fraction were then analyzed by SDS-PAGE followed by western blotting using HDAC-2 and 3-specific antibodies as well as a histone H1-specific antibody as a loading control.

RNA Analysis by qRT-PCR of Parental and DTP Cells

Total RNA was isolated using the RNeasy kit (Qiagen) following the manufacturers' directions and subjected to DNase treatment. For analysis by Fluidigm, isolated RNA was subjected to a one-step cDNA synthesis using the iScript cDNA synthesis kit (Bio-Rad) and subsequent pre-amplification using the Taqman PreAmp Mastermix (ABI 4391128) according to the manufacturer's protocol, with the exception that PCR cycling conditions were modified to a 14 cycle pre-amplification step. Following amplification, samples were diluted 1:4 with TE buffer and qRT-PCR was conducted on Fluidigm 96.96 Dynamic Arrays using the BioMark™ HD system according to the manufacturer's protocol. Probes used for Fluidigm were G9a/EHMT2 (Hs00198710_m1), GAPDH (Hs02758991_g1), GLP/EHMT1 ((Hs00964325_m1), Suvar39H1 and H2 ((Hs00957892_m1 and Hs00226596_m1), SETDB1 (Hs01048361_m1), EZH2 (Hs00544830_m1), EZH1 (Hs00940463_m1), EED (Hs00537777_m1), suz12 (Hs00248742_m1) and Jarid2 (Hs01004467_m1). All probes were purchased from Life Technologies.

Sample Generation for RNA Studies

For studies in parental PC9 cells, cells were either treated with 1 μM erl (24 hours), 50 μM carboplatin (carb, 72 hours) or 50 nM TSA (5-6 hours as indicated). For PC9DTPs, 4 day DTPs were treated with 50 μM carboplatin (72 hours) or 50 nM TSA (5-6 hours as indicated). ERCC RNA spike-in mix 1 (Ambion 4456740) was added based on the ratio of total cell number to total RNA (1 μL of

1:10 diluted spike-in mix to $2x10^6$ cells). After which RNA was prepared as described above and subjected to qRT-PCR or RNAseq analysis.

LINE-1 RNA Analysis by Taqman

For analysis of LINE-1 expression using Taqman, RNA was isolated as above and ERCC RNA spike-in mix 1 (Ambion 4456740) was added based on the ratio of total cell number to total RNA (1 μL of 1:10 diluted spike-in mix to $2x10^6$ cells). Taqman Fast Virus 1-Step master mix for qRT-PCR was used in a ViiA 7 qRT-PCR machine (Applied Biosystems). For qRT-PCR, 10 ng total RNA was subjected to a 15 minutes RT reaction at 48°C followed by a 20 second inactivation/denaturation at 95°C. Samples were then subjected to 40 cycles of 3 seconds at 95°C followed by one minute at 60°C. Samples were run in triplicate and cycle threshold (Ct) values were converted to relative expression values using β-actin, or ERCC spike-in as internal controls. LINE-1 probes used:

L1-5'UTR-1 (Coufal et al., 2009):
Forward: 5'-GAATGATTTTGACGAGCTGAGAGAA-3'
Reverse: 5'-GTCCTCCCGTAGCTCAGAGTAATT-3'
Probe: 5'-AAGGCTTCAGACGATC-3'
L1-5'UTR-2 (Wissing et al., 2012):
Forward: 5'-ACAGCTTTGAAGAGAGCAGTGGTT-3'
Reverse: 5'-AGTCTGCCCGTTCTCAGATCT-3'
Probe: 5'- FAM-TCCCAGCACGCAGC-BHQ-3'
L1-ORF1 (Wissing et al., 2012):
Forward5'-TCAAAGGAAAGCCCATCAGACTA-3'
Reverse 5'-TTGGCCCCCACTCTCTTCT-3'
Probe: 5'- FAM-CAGCGGATCTCTCGG-BHQ-3'
L1-ORF2 (Wissing et al., 2012):
Forward: 5'-GGATGGCTGGGTCAAATGGT-3'
Reverse: 5'-GAGAGGATGCGGAGAAATAGGA-3'
Probe: 5'-FAM-CAACCATTGTGGAAGTCAGTGTGGCG-BHQ-3'

Probes from Life Technologies for ERCC RNA spike-in mix 1 (Ac03459872_a1) and β-actin (Hs01060665_g1) were used for normalization as indicated in the figures.

LINE-1 RNA Analysis by SYBR Green qRT-PCR

Real-time cycling and analysis was performed with an ABI ViiA7 instrument in 384-well format using a SuperScript III Platinum SYBR Green One-Step qRT-PCR Kit with ROX (Invitrogen). For qRT-PCR, 10 ng total RNA was subjected to a 15 minutes RT reaction at 50°C followed by a 5 minute inactivation at 95°C. Samples were then subjected to 40 cycles of 15 seconds at 95°C followed by two minutes at 60°C. Samples were run in triplicate and cycle threshold (Ct) values were converted to relative expression values using β-actin as the housekeeping marker. These are the specific primers used for quantification of LINE-1 transcripts:

L1-ORF1-1 (Guo et al., 2014):
Forward: 5'- TCAAAGGAAAGCCCATCAGACTA -3'
Reverse: 5'- TGGCCCCCACTCTCTTCT -3'
L1-ORF1-2 (Chen et al., 2012):
Forward: 5'- GGTTACCCTCAAAGGAAAGCC -3'
Reverse: 5'- GCCTGGTGGTGACAAAATCTC -3'
L1-5'UTR (Guo et al., 2014):
Forward: 5'- ACGGAATCTCGCTGATTGCTA -3'
Reverse: 5'- AAGCAAGCCTGGGCAATG -3'
L1-ORF2 (Chen et al., 2012):
Forward: 5'- AAATGGTGCTGGGAAAACTG -3'
Reverse: 5'- GCCATTGCTTTTGGTGTTTT -3'
β-actin (Guo et al., 2014):
Forward: 5'- GGCATGGGTCAGAAGGATT -3'
Reverse: 5'- GGGGTGTTGAAGGTCTCAAA -3'

Taqman Analysis of IFN Response/Antiviral Defense Genes

For this analysis RNA was isolated as described above. Taqman Fast Virus 1-Step master mix for qRT-PCR was used in a ViiA 7 qRT-PCR machine (Applied Biosystems). For qRT-PCR, 10 ng total RNA was subjected to a 15 minutes RT reaction at 48°C followed by a 20 second inactivation/denaturation at 95°C. Samples were then subjected to 40 cycles of 3 seconds at 95°C followed by one minute at 60°C. Samples were run in triplicate and cycle threshold (Ct) values were converted to relative expression values using β-actin as an internal control. Probes were purchased from Life Technologies for Rig-1/DDX58 (Hs01061436_m1), IFIH1: (Hs00223420_m1), IRF7: (Hs01014809_g1), OASL: (Hs00984387_m1) and β-actin probe used as internal standard (Hs01060665_g1).

Patient Samples and RNA Analysis from Tumor Tissues

BRIM2 (NCT00949702) was a single-arm phase 2 clinical study in which patients with metastatic melanoma carrying a BRAFV600E mutation received vemurafenib. The data cutoff used in the analyses herein was in February 2012. Pretreatment (archival or baseline) tissue blocks were available from 64 of 132 (48%) patients from BRIM2. For 18 patients, tissue biopsy blocks taken on day 15 of continuous vemurafenib treatment were available in addition to a pre-treatment sample. Patient consent was obtained for exploratory research conducted on all tissues. mRNA was prepared from FFPE sections of tumor tissues and gene expression was measured using Nanostring. Data were normalized to the geometric mean of all 800 genes measured. The effect of baseline expression was determined using a Cox proportional hazards model. Treatment effect was compared between PR and PD/SD patients using a t-test.

HPLC Separation of Histone Variants

Nuclei from PC9 cells were isolated as described (Mendez and Stillman, 2000). Histones were prepared from the nuclei by acid extraction and enriched by reverse-phase HPLC as previously described (Shechter et al., 2007). Briefly, cells were harvested and lysed in 10 mM HEPES, 10 mM KCL, 1.5 mM $MgCl_2$, 0.34 M sucrose, 10% glycerol, 1 mM DTT, protease and phosphatase inhibitors and 1% Triton X-100. The extraction mixture was centrifuged at 1300 x g for 4 minutes and the nuclear pellet was recovered and acid extracted with 0.4 M $NH4_2SO_4$ and TCA-precipitated. The histone pellet was solubilized in 0.1% TFA and loaded onto a C8 reverse-phase column (Aquapore RP-300, Perkin Elmer) equilibrated with 0.1% TFA/5% ACN. Histones were eluted with a gradient of 90%ACN/0.1% TFA. Fractions for histone peaks were pooled (see Figure S3J for example) and analyzed by MS.

Preparation of Histones for Mass Spectrometry

HPLC-separated histones were prepared as described above. For all other mass spectrometric analyses histones were extracted and purified from frozen pellets of 5 million cells each using a commercial kit (Histone Purification Mini Kit; Active Motif, Carlsbad, CA). In both cases, purified histones were prepared for MS by lysine-propionylation, trypsin digestion and N-terminal labeling with phenyl isocyante as previously described (Maile et al., 2015). Briefly, histones were reacted with propionic anhydride under mild aqueous conditions to block the ε-amines of all unmodified or mono-methyl lysines. Digestion with trypsin thereby yielded arginine-terminated peptides, whose neo n-termini were then labeled with phenyl isocyanate. After desalting on C18 "StageTips" the histone peptides were eluted into autosampler vials for mass spectrometric analysis. Stable isotope labeled internal standards were introduced in the form of SILAC-labeled core histones isolated from PC9 cells (mixed prior to propionylation) (Maile et al., 2015), or as pooled standards labeled with $^{13}C_6$ phenyl isocyanate (mixed prior to StageTip desalting) (Vinogradova et al., 2016).

Histone H3PTM Analysis by Mass Spectrometry

Histone peptides were fractionated by reverse-phase capillary HPLC in-line with the microelectrospray source of a hybrid ion trap-orbitrap mass spectrometer: either an Orbitrap-Elite or Orbitrap-Fusion (Thermo Scientific). Detailed chromatographic and operating conditions for the two instruments have been previously described (Maile et al., 2015; Vinogradova et al., 2016). Data were acquired in parallel-reaction monitoring experiments that targeted peptides from histone H3 in their various combinations of post-translational modifications; see supplementary tables for the specific peptides targeted in each experiment. Quantitative data were extracted from the mass spectra as peak areas using the Skyline application (MacLean et al., 2010) and converted to relative abundance by peptide and histone mark with inter-sample normalization via the stable isotope labeled internal standards as previously described (Maile et al., 2015). Fold changes were calculated as $\log_2$ ratios with respect to the relevant control.

ATACseq Data Generation

Cultured cells were detached using TrypLE (Life Sciences), counted, resuspended in growth media containing 5% DMSO and then aliquoted in cryovials containing 75,000 viable cells/vial. Cells were frozen and stored in -80C prior to processing for ATACseq. ATACseq was performed as described (Buenrostro et al., 2013). DNA libraries were sequenced using Illumina HiSeq 2500 at 50 bp paired end reads.

ChIPseq Data Generation

PC9 parental cells and DTPs untreated or treated with 50 nM TSA for 5 hours were fixed with 1% formaldehyde for 10 minutes at room temperature. To stop the reaction, glycine was added to a final concentration of 0.125 M. Fixed cells were washed 3 times with PBS. Chromatin was isolated by the addition of a standard lysis buffer containing 600 mM NaCl. DNA was sheared by sonication to 300-500 bp size fragments. For genomic DNA controls (input controls) the chromatin was treated with RNase and Proteinase K followed by reversal of the crosslinking and ethanol precipitation. DNA was quantified using a NanoDrop spectrophotometer. For ChIPs, a 30 μg aliquot of chromatin was pre-cleared by incubation with protein Agarose beads (Invitrogen). Chromatin was immunoprecipitated with anti-H3K9me3 (abcam ab8898) or anti-H3K4me3 (Cell Signaling 9751) antibody in the presence of 0.4 μg H2Av antibody (Active Motif 39715) and 750 ng of sonicated *Drosophila* chromatin. After extensive washing with ChIP buffer, the chromatin was eluted from the beads with SDS buffer. The immuno-precipitated chromatin was treated with RNaseA and Proteinase K and crosslinking was reversed by overnight incubation at 65°C. ChIP DNA was purified by phenol-chloroform extraction and ethanol precipitated. Illumina sequencing libraries were prepared from the ChIP and input DNAs. The resulting DNA libraries were quantified and sequenced as 150 bp paired-end reads using Illumina's HiSeq 2500 (fragments had average lengths of about 500 bp).

RNAseq Data Generation

For studies in parental PC9 cells, cells were either treated with 1 μM erl (24 hours as indicated), 50 μM carboplatin (72 hours) or 50 nM TSA (5-6 hours as indicated). For DTPs, 4d DTPs were either untreated or treated with 50 nM TSA (5-6 hours as indicated). The number of hours chosen for erl and carboplatin treatment represent a time before extensive ablation of the parental population has occurred (however, there are cell cycle effects on the population at this time). Thereafter, RNA was prepared as described above and subjected to qRT-PCR or RNAseq analysis. A common set of external RNA controls has been developed by the External RNA Control Consortium (ERRC, ambion: 4456740), hosted by the National Institute of Standards and Technology (NIST). The ERCC mix was diluted 1:10 and 1 μl was added to total RNA from 2 million cells. Data were collected using 150 bp paired-end read (PE150) sequencing of mRNA isolated from samples above (at Expression Analysis Inc).

QUANTIFICATION AND STATISTICAL ANALYSIS

For all experiments p values were calculated using PRISM7 graphpad paired t-test, unless otherwise noted (n.s.>0.05, *<0.05, **<0.01, ***<0.001, ****<0.0001).

ATACseq Analysis

Sequencing reads were aligned to human genome build hg19 using Bowtie (Langmead et al., 2009) with essentially the same parameters as described previously (Buenrostro et al., 2013), except when the reporting parameter was changed from -m1 to -M1 in order to include a randomly selected single alignment for reads mapping to multiple locations. For experiments presented in Figures 4F, 4G, and S4A–S4G alignments were done using BWA version 0.7.12 and peaks were detected using MACS 1.4.2 with p-value 1e-7 and no model option (Gal-Yam et al., 2008). Peak filtering was performed by removing false peaks in the ENCODE blacklist (The Encode Project Consortium, 2012). Peaks obtained from triplicate samples for each experimental condition were merged. For each sample the distribution of fragment lengths was determined based on the distance between paired-end sequences reported during alignment. The distribution was normalized based on the total number of fragments in each sample to calculate the percentage of fragments from 30 to 2000 bp in length. Differential fragment lengths between samples were presented as the $\log_2$ ratio of the percentage of fragments of each size displayed along x-axis. Genome-wide accessibility data was calculated using a 150 bp sliding window (step size = 20 bp) to calculate the number of overlapping paired-end fragments. The paired-end fragments were represented as the coordinate for the first and last base of the fragment, which correspond to the accessible bases. All samples were normalized to the total number of reads per 10 million reads sequenced and converted to bigWig format using the software available from UCSC (Kent et al., 2010). Additional details regarding analysis can be found in the Supplemental figure legends.

ChIPseq Analysis

For analysis, sequencing reads were aligned to human genome build hg19 with BWA using default parameters (Li and Durbin, 2010). Resulting BAM files were filtered to extract only reads that belonged to matching pairs; pairs of reads that spanned on the average ~350-400 bp and were in the correct orientation. Read pairs with mapping quality 0 (high quality mappings to multiple locations) were not used for further analysis; in addition, presumptive PCR duplicates and reads that did not pass Illumina's purity filter were removed. Total number of reads was normalized according to the total number of reads that map to the *Drosophila* dm3 genome from each sample. H3K9me3 and H3K4me3 ChIPseq peaks were called with SICER using input files as control (Zang et al., 2009). PC9 parental and DTP peaks were annotated according to genomic features using HOMER (homer.salk.edu). Coverage files were generated by extending reads to 380 bp in silico and counting tags for 50-nt bins over the genome. Repeat annotations were retrieved from RepeatMasker track using UCSC Table Browser (Karolchik et al., 2004). IGV genome browser was used to view Genomic regions. SeqPlots was used to generate and visualize signal intensity matrices over 10 kb genome intervals that are centered around LINE-1 elements that overlapped with a H3K9me3-peak as heatmaps and line plots (Stempor and Ahringer, 2016). For the analysis of H3K9me3 Chipseq reads in telomeric and centromeric repeats, the sub-telomeric sequences were collected (Stong et al., 2014) and the centromere and satellite sequences were derived based on the genomic coordinates from the UCSC genome browser (human genome assembly GRCh38). H3K9me3 ChIPseq reads were first filtered to remove reads with low sequencing quality and reads aligned to ribosomal DNA sequences. The remaining "high quality reads" were aligned to the collection of sub-telomere, centromere and satellite sequences using GSNAP (Wu and Nacu, 2010). Numbers of reads mapped to these repeat sequences (including reads mapped to multiple locations and reads with only one of the two ends mapped) were counted for each sample. Percentages of pooled reads mapped to sub-telomeric and centromeric repeats were calculated as presented in Figure S5B.

RNAseq Analysis

In order to quantify transcripts, repeats and ERCC spike-ins, Salmon (Patro et al., 2017) was used. The set of transcripts used for making an index (fmd index) for Salmon included I. refseq transcripts that were adapted to reflect the genomic sequence (GRCh38 build genome, 90287 sequences), II. repeat masker annotated regions of the human genome (http://hgdownload.cse.ucsc.edu/goldenPath/hg38/database/rmsk.txt.gz, 5099101 sequences), and III. ERCC sequences (92 sequences). Salmon-based quantification of expression values for these sequences was then rolled up for unique genes (30727 genes total) across transcripts from the same gene. Similarly, for repeats, expression values were aggregated at several levels, including family (n=157), class (n=67)

and repeat names (n=17319). For normalization of rolled up expression values, several normalization factors were considered that assumed equal median expression values across expressed genes, repeats, repeat families, or ERCC spike-ins. The normalization factors were obtained using the 'RLE' method of the calcNormFactors function the Bioconductor package edgeR (Robinson et al., 2010). These were then converted into size factors by multiplying by the library sizes. Correlation of gene-based size factors was weak with repeats and repeat families (Pearson correlation coefficient 0.659 and 0.649 respectively), and even weaker with ERCC spike-ins (0.447). However, due to the potential global nature of expression changes in this study, we selected ERCC-based normalization of the expression values of genes and repeats. ERCC-normalized expression data was then used for differential expression analysis using the voom-limma approach (Law et al., 2014). Multiple testing corrections were performed using the Benjamini-Hochberg method.

DATA AND SOFTWARE AVAILABILITY

The ATACseq, RNAseq and ChIPseq data has been deposited to Geo: GSE74180 data upload [NCBI tracking system #18446588]
The Histone MS data has been deposited to: http://www.peptideatlas.org/PASS/PASS01054.